THE PENNSYLVANIA STATE UNIVERSITY
COLLEGE OF ENGINEERING

NGR-39-009-023

SYSTEMS AND CONTROLS LABORATORY

RESEARCH REPORT NO. 9 UNIVERSITY PARK, PA. APRIL, 1969

THE SYSTEMS AND CONTROLS LABORATORY

The Systems and Controls Laboratory was started in 1964 to encourage graduate research and development on engineering systems, with emphasis on improving the understanding of basic elements and devices and bridging the gap between theory and practice. The experimental equipment and facilities of this laboratory have been provided for carrying out experimental investigations on devices and systems involving many of the different engineering disciplines. Staff members, graduate fellows and graduate assistants are now working on projects and thesis topics of vital interest to engineers concerned with the advanced design and development of new engineering systems.

Much of the work involves mathematical and computer modeling and analysis and the experimental investigation of breadboard and prototype systems or devices. A major goal of this work is to accomplish a useful synthesis of analytical and experimental methods in research and development of advanced engineering systems for effective use by engineers and scientists working on future aerospace systems.

Financial support for this program is derived from the University, The National Aeronautics and Space Administration, The Bell Telephone Laboratories and the Optimizer Control Corporation. A major share of the projects in the Systems and Controls Laboratory are supervised by Dr. J. L. Shearer, Rockwell Professor of Engineering and Dr. A. J. Healey, Assistant Professor of Mechanical Engineering, assisted by other members of the graduate faculty.

CONTENTS

SPREADING OF JETS IN FLUID AMPLIFIERS

J. L. Shearer, Rockwell Professor of Engineering

The study of the effects of jet supply conditions on the spread rate of a jet in a fluid amplifier, discussed in earlier progress reports has now been completed with the submission of an M. S. thesis by R. W. Gray [9]* The results of this thesis reveal some of the effects of high levels of upstream turbulence on the velocity and turbulence profiles in the idealized mixing region (up to 10 nozzle widths downstream) of a semi-confined jet. This results in a better understanding of the events which occur in the control port interaction regions of fluid amplifiers and fluid logic devices. This summary of Gray's work is taken from his thesis.

The development of a jet issuing from a rectangular nozzle and confined by top and bottom plates was studied for changes in upstream disturbance intensity. The upstream disturbance intensity, observed as the exit (centerline) rms intensity, was changed by introducing high velocity secondary flows upstream of the converging nozzle, thereby inducing eddies within the jet.

The first part of the study consisted of a survey of the horizontal centerplane velocity and turbulence intensity profiles of an essentially two-dimensional flow: the flow from a nozzle of aspect ratio (ratio of height to width) 8:1. It was found that the horizontal midplane velocity profiles in the idealized mixing region, from about one to 10 nozzle widths downstream of the nozzle exit plane, could be normalized onto a common profile with the geometrical similarity as illustrated in Fig. 1. The self-preserving geometry is revealed by using the parameter η to describe radiating lines of constant normalized velocity in the mixing region, with η defined by:

$$\eta = \frac{Y-\varepsilon}{X-X_o}$$

where the origin of the idealized mixing region (origin of lines of constant η) is displaced from the edge of the nozzle by the coordinates X_o and ε. The correction ε, which is of the order of magnitude of the displacement thickness of the boundary layer at the nozzle exit plane, is a function of initial flow conditions. This correction is required to normalize data near the nozzle exit. The constant X_o is the distance of the virtual origin of the mixing layer from the nozzle exit plane and it is determined experimentally as the correction necessary to best normalize the velocity profiles near the nozzle onto a common profile. The parameter X_o may be several hundred exit boundary layer thicknesses upstream or downstream of the exit plane.

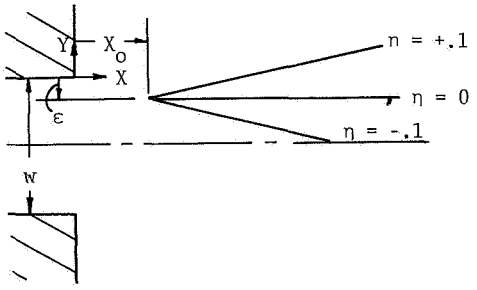

a) Geometrical Representation

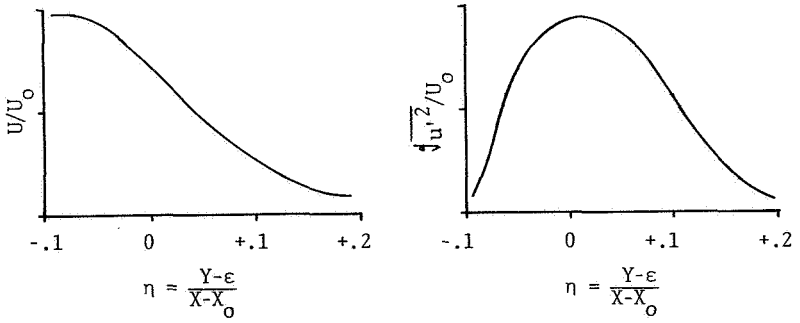

b) Normalized Velocity Profiles and rms Intensity Profiles

Fig. 1 Self-Preservation in the Idealized Mixing Regions

*Nos. in parentheses denote references at end.

Qualitatively, the effect of increasing the exit rms intensity was to change the boundary layer thickness leaving the nozzle and thus to change the value of ε slightly and to change X_o, shifting the virtual origin slightly upstream for small increases in the exit rms intensity and then downstream again for larger increases in the exit rms intensities. However, for a given geometry it was found that the dimensionless spread rate decreased with increasing exit velocity. Changing the upstream geometry also changed the dimensionless spread rate.

The normalizing of data in the idealized mixing regions (i.e. both sides of the jet) onto a single profile allows the flow in the mixing regions to be well described by the maximum dimensionless slope (the dimensionless spread rate), the virtual origin of the idealized mixing layer, and the velocity at $\eta = 0$, which is constant for approximately twice the length of the core of the jet (about 10 nozzle widths). The entire jet, including the asymptotic jet, can be described by these parameters if the local velocity is nondimensionalized with respect to the velocity at $\eta = 0$ at the same axial distance. This procedure is analogous to nondimensionalizing with respect to the centerline velocity to normalize data, as is classically done on the asymptotic jet.

The changes in the virtual origin with exit rms intensity noted above are similar to those noted by Bradshaw [10] when he lengthened the straight section downstream of the contraction in a round nozzle. This similarity suggests that a major part of the influence of the exit rms intensity is due to its changing the exit boundary layer, that a major effect of lengthening the straight section of a nozzle is to increase the exit rms intensity, or that some other parameter such as the Reynolds stress is affected similarly by both changes in upstream conditions.

Several tests were made at the centerline of flows both at aspect ratios of 8:1 and 4:1. It was found that increasing the exit rms intensity decreases the length of the core of the jet, and that this effect seems more pronounced at the lower aspect ratio.

Decreasing the exit centerline velocity decreases the core length. The exit plane boundary layer profiles over a 5:1 range of exit velocity were similar and showed a decrease in thickness with increasing velocity. The boundary layer at the exit grows thicker with increasing exit rms intensity, but these exit plane boundary layer velocity profiles have non-similar shapes. Decreasing the exit centerline velocity and increasing the exit rms intensity both show a shorter core and a thicker boundary layer. Turbulence measurements were self-preserving out in the idealized mixing regions however.

The second part of this study consisted of a survey of three-dimensional spreading with a nozzle having an aspect ratio of 4:1. It was found that the profiles in the horizontal centerplane of a low exit rms intensity flow was not self-preserving using the similarity geometry based on the parameter η. However, the velocity profiles in a higher exit rms intensity flow were self-preserving. The effect of increasing the exit rms intensity on the development of the velocity profile in the vertical centerplane was to change the velocity profile from one with the highest velocity at the centerline to one with peaks near the upper and lower confining plates. Measurements in a plane parallel to the exit plane confirmed this observation of significant velocity peaks near the plates for a higher exit rms intensity flow. These latter results reveal additional information regarding secondary flow effects with lower aspect ratios, reported earlier by Foss and Jones [11] and Bettoli [12], especially when higher turbulence levels are present in the nozzle.

As each boundary layer at the nozzle exit was usually 20% or more of the half width of the nozzle, care must be taken in relating the results of this study to most other studies which minimize boundary layer effects. However, the results are very applicable to miniature devices like fluid amplifiers in which the boundary layer is a large part of the nozzle half width.

More details of this work are available in the complete thesis.

These studies were supported by NASA Grant No. 39-009-023.

THERMAL SWITCHING OF JET FLOWS

J. L. Shearer, Rockwell Professor of Engineering

Much of the work done on this project has been described in earlier reports. However, this project has now been completed with the submission of a Doctoral thesis by R. E. Tomek [13]. In the final phases of this work the experimental investigation of a large size model was completed and attempts were made to apply and extend the theory of turbulent flow to semi-confined wall jets. Although the objective of trying to derive a mathematical model for use in the design of a thermally-switched jet device was not achieved, enough experimental data was obtained to design a small size model shown in Figs. 2 and 3. The small size model worked reasonably well, although the response time was much longer than hoped for; and the heat flux rate (heater power per unit wall area) had increased by a factor of 10, possibly because of heat lost to the walls of the device. Although it appears that this work should be extended to studies of thermal switching with curved wall diffusers, it is most important to gain a better understanding of the turbulent flow phenomena associated with semi-confined wall jets so that unsteady fluid flow and heat flow effects may be properly modeled.

An interesting by-product of this work has been the oscillating vane-digital output flow rate sensor subsequently investigated by M. B. Song.

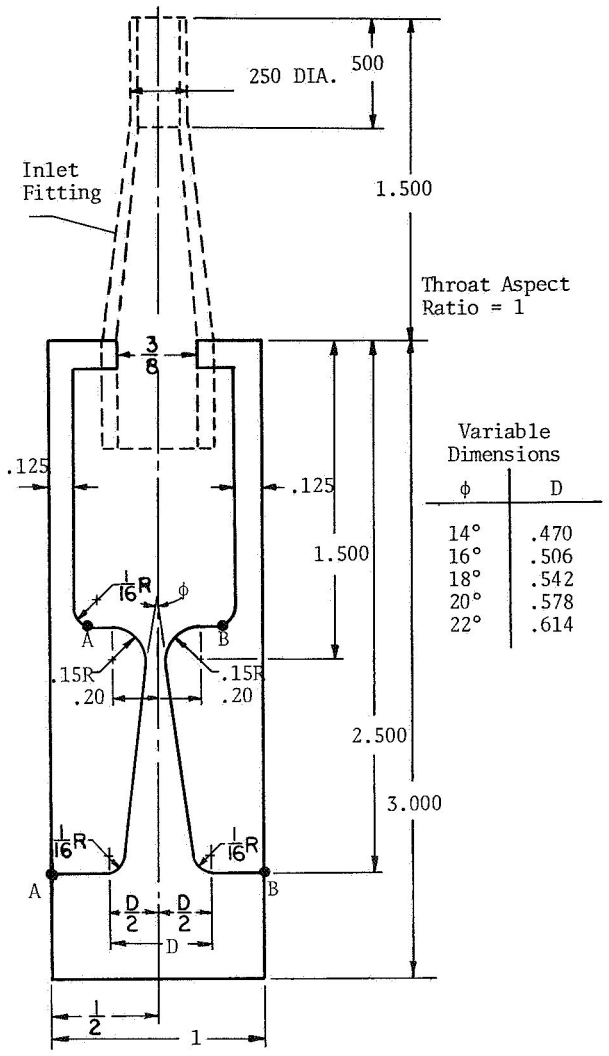

Fig. 2 Dimensions of the Small Diffuser Test Models

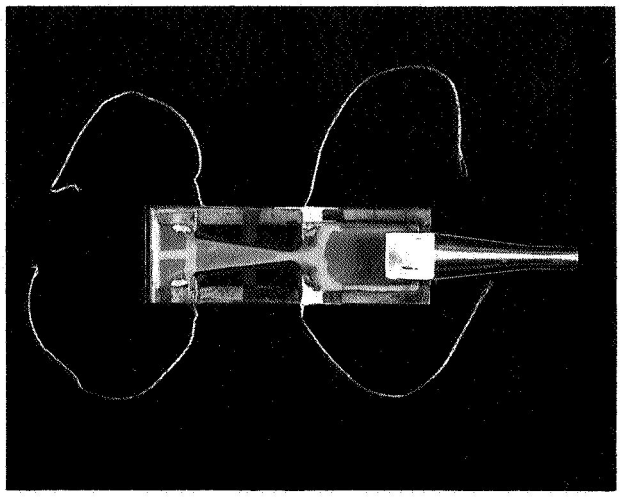

Fig. 3 Top View of a Small Diffuser Test Model

The Preceeding work was supported in part by NASA Grant NGR 39-009-023.

FLUIDICS REFERENCE CENTER

M. R. Fahnestock, Research Assistant in M. E.

During the past decade the field of Fluidics has grown rapidly, and the volume of literature that has emerged from this expansion has grown with equal vitality. As a consequence, it has become increasingly difficult to make a comprehensive search of the existing material and arrive at the relevant information. Even the most ardent student of Fluidics has been hard pressed to keep abreast of new techniques and developments. The end result has been a communications gap between the research engineer and, in particular, the industrial engineer. This communications gap has caused Fluidics to be misunderstood, if not mistrusted, in many instances. The Fluidics Reference Center (FRC) is an outgrowth of the concern for this problem. The FRC will provide a readily accessible bank of literature and information pertinent to Fluidics. Even more significant, the information will be ordered in such a manner that a user should encounter little difficulty locating a paper that is relevant to his interest. He will be able to conduct his search manually, i.e., leaf through the files himself; or if a sophisticated or rapid search is desired, a computer routine will facilitate such a search. The user's output from the Reference Center will be a bibliography of appropriate references plus abstracts of the most pertinent ones. It is not the intent of the FRC to supply copies of complete papers. This service would normally be handled through a library.

At this writing only a small percentage of the available reference material is entered into the system. This is due to the comprehensive indexing technique employed before a paper is entered. Besides the normal indexing one might expect such as author and title files, the Reference Center will also incorporate files such as location of the lead author, chronological order of publication, and most important, an area code file. For the area code file, various aspects of Fluidics and related subjects are separated into main areas (up to 26) and then each main area is divided and sub-divided into appropriate subareas (up to 36 for each). Hence, each incoming paper is read and then assigned area code numbers (up to five) for cross-indexing. As this coded bank of information is accumulated, it is being stored on magnetic tape for purposes of reproduction and/or rapid print-out (magnetic tape, hard copy, papertape, tabulating cards) and for computerized information retrieval.

The extra effort and talent required for this form of indexing is justified by the additional flexibility afforded to the user in selecting references in a specific area of Fluidics. Use of the area codes makes manual searching not only possible but convenient. Furthermore, this approach reduces the number of superfluous references turned up by a given search. By making judicious use of the index filed and/or the computer, a user will be able to quickly and efficiently select from the volume of existing literature the papers which are most meaningful.

At the present time the FRC is beginning to emerge from the early stages of its evolution. Considerable time and effort was required to develop a functional indexing system for cataloging the literature. This now exists, and furthermore, the index system is open-ended allowing additions or expansions to the system as future needs may dictate. The information retrieval program for the computer is now functional; although some refinements are needed and productive efforts in this area are continuing.

This project has been funded by the College of Engineering and the Conference Center of The Pennsylvania State University.

NOZZLE THRUST MODULATION BY VORTEX GENERATION

T. D. Gillespie, Research Assistant in M. E.

In conjunction with this project, a trip was made to the NASA Ames Research Center, March 24 - 26, 1969 in order to discuss potential applications of this concept and to determine what support would be available for conducting research work at that facility on this project.

Through contacts with G. Allen Smith, of Guidance and Control Systems, as well as Mark Kelly and other personnel of the 40 x 80 Wind Tunnel, arrangements were made for a test program of 10 to 12 weeks duration beginning in September of this year.

Continuation of the research discussed in the previous report [8] has been concerned with development of an instrumentation package suitable for determining the flow conditions including necessary thermodynamic properties existing at the throat of the nozzle under swirling flow conditions. Since the flow should be sonic or near sonic at the throat, the instrumentation must be of a unique character. In addition, the very directional nature of the flow and the necessity of measuring all quantities in the plane of the throat imposes further restrictions on the instrumentation. In anticipation of the difficulties common to flow measurement in this velocity range, some redundancy in the instrumentation is planned as a check on the validity of the measurement techniques.

Among the components selected for the instrumentation package is a "vortex meter" developed in the Aeronautical Engineering Department at this university. The vortex meter, shown in Fig. 4, consists of two perpendicular fins mounted on a shaft supported by jewel bearings. Rotation of the fin-shaft assembly is detected by an optical pickup. In the absence of friction the fins will rotate at the speed of rotation of the fluid stream in which it is immersed. The actual frictional characteristics, however, are related to the relative velocity of the fin-shaft assembly in the housing and the dynamic load developed by the axial flow over the fins and must, therefore, be determined by calibration. Since a flow with near sonic axial velocity and a known rotation parallel with the axial direction

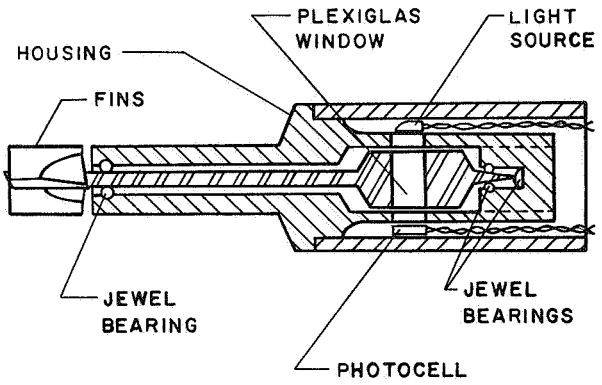

Fig. 4 Cross Section of the Vortex Meter

is difficult to achieve, calibration was attempted in a non-rotating high speed flow by rotating the meter housing. It was discovered that speeds above 5000 to 8000 rpm caused the oil to spin off of the jewel bearings, and reliable calibration in the expected range of operation, 15,000 to 30,000 rpm, was impossible.

During the early part of this report period the Ingersoll-Rand air compressor, which supplies the air for this project, became inoperable. Investigation revealed failure of all the rings on the second stage compressor which subsequently caused extensive internal damage to the unit. After four months the Ingersoll-Rand Company has not yet been able to accomplish the needed repairs. Therefore, testing on this project has been curtailed indefinitely at this location.

Analytical studies of swirling compressible flow through a converging nozzle are continuing.

These studies are supported by NASA Grant No. NGR 39-009-023.

Oscillating Vane-Digital Flow Rate Sensor

M. B. Song, Graduate Student in M. E.

A recently proposed method of oscillating vane-digital flow rate sensing was studied experimentally to find the relationships between the passing air flow rate and the vibration frequency of an oscillating vane in a two-dimensional converging-diverging passage. A first progress report appears in the previous report [8].

Throughout all measurements, the following should be considered:

1. Frequency measurements were obtained from an electronic counter accumulating pulses over a ten-second interval. These measurements were accurate to within .1 cps.

2. Pressure readings by water column manometer were made in order to indicate the average value of fluctuating pressures at several points in the model.

3. The fluid temperature was measured immediately downstream of the nozzle throat.

4. Flowmeter readings were converted into scfm (standard cubic feet per minute) employing corrections for temperature and pressure recommended in the Handbook of the Variable Area Flowmeter [14]. Since the standard conditions at Fischer and Porter Co., refer to 14.7 psia and 70°F, the maximum scfm of the flowmeter employed in this work (100% = 6.8 scfm air when metered at 11.2 psia and 100°F) was corrected as follows:

$$6.8 \times \sqrt{\frac{14.7}{11.2}} \times \sqrt{\frac{560}{530}} = 8.0 \text{ scfm}$$

In order to further study the major phenomena, including discontinuity phenomena of the oscillating vane-device as a flow rate sensor, the original test model was slightly modified by adding several pressure taps along the centerline of the top plane and one side of the diffuser wall as shown in Fig. 5. Both a water column manometer and pressure transducer were employed for these measurements.

It has been found experimentally that by releasing the vane from any stationary position between the two contact points of the test model except the exact centerline of the passage, the vane will start to move toward the opposite side of the centerline; and whenever there exists a considerable amount of flow, it will even start oscillating from the centerline position (see Fig. 5).

Once it starts to move in this way, it will oscillate and quickly reach full amplitude α. It is evident that the unsteady fluid flow phenomena on both sides of the vane result in a net increment in the kinetic energy of the vane during each stroke, which is apparently dissipated during the impact at the end of each stroke.

The main tests have been carried out in two separate cases, identified as Case I and Case II (rotating centers of which are I and II respectively in Fig. 6). In addition, some special tests have also been performed to investigate the specially-arranged geometry of a test model identified as Case III (but most of the tests and analysis were made for Case I).

From the tests carried out so far, quite linear relationships (with wide range -- over 13:1) between flow rate and oscillating frequency were obtained in certain cases as shown in Fig. 7. However, it should be noted that the discontinuity phenomena appears in the relatively higher range of oscillating frequency for most operating conditions and various geometries of the test model employed. Fig. 8 shows an example of this.

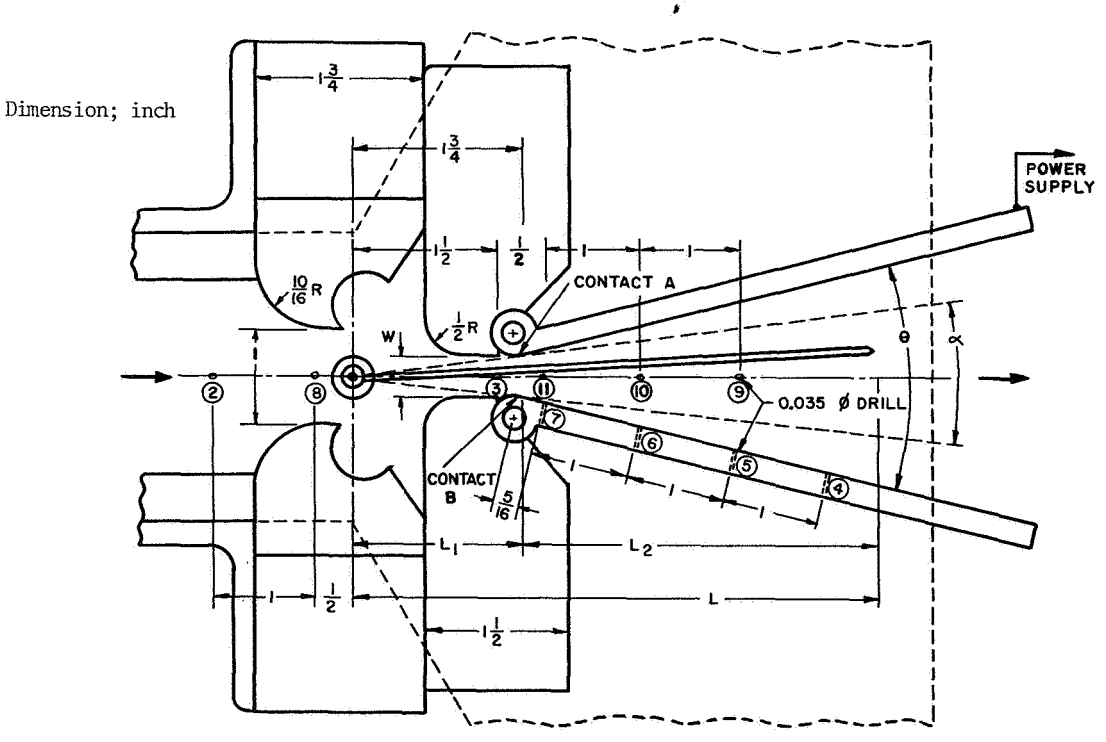

Fig. 5 Typically Arranged Test Model -- Case I

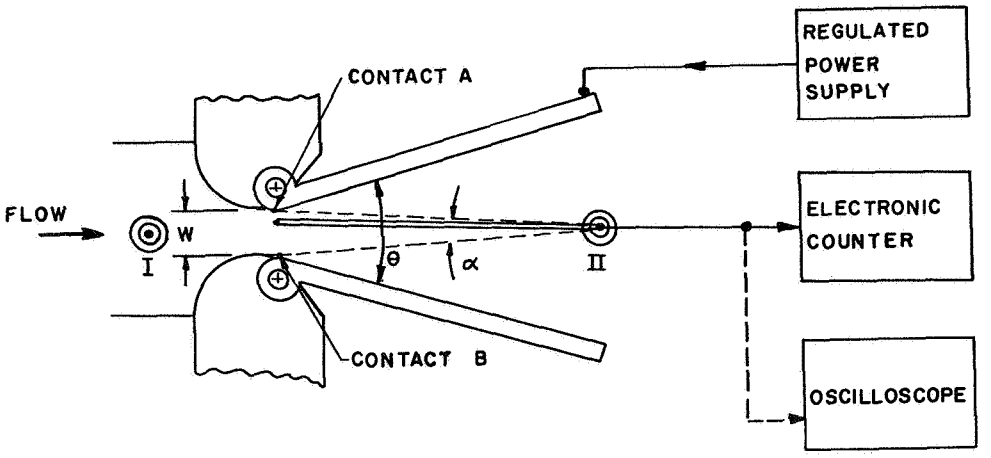

Fig. 6 Schematic Showing Operating Principle of the Oscillating Vane-Device

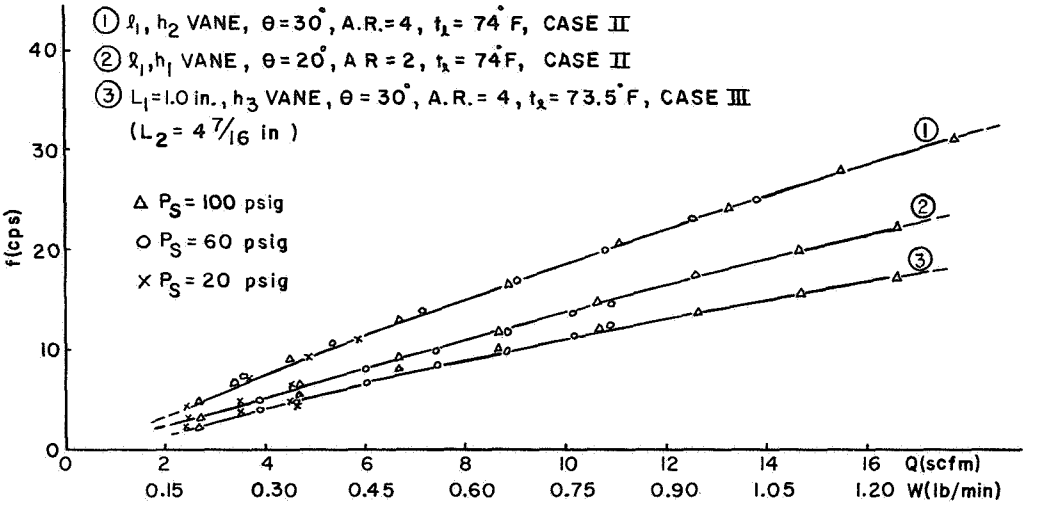

Fig. 7 Examples Showing Linear Relationships Between Flow Rate and Oscillating Frequency

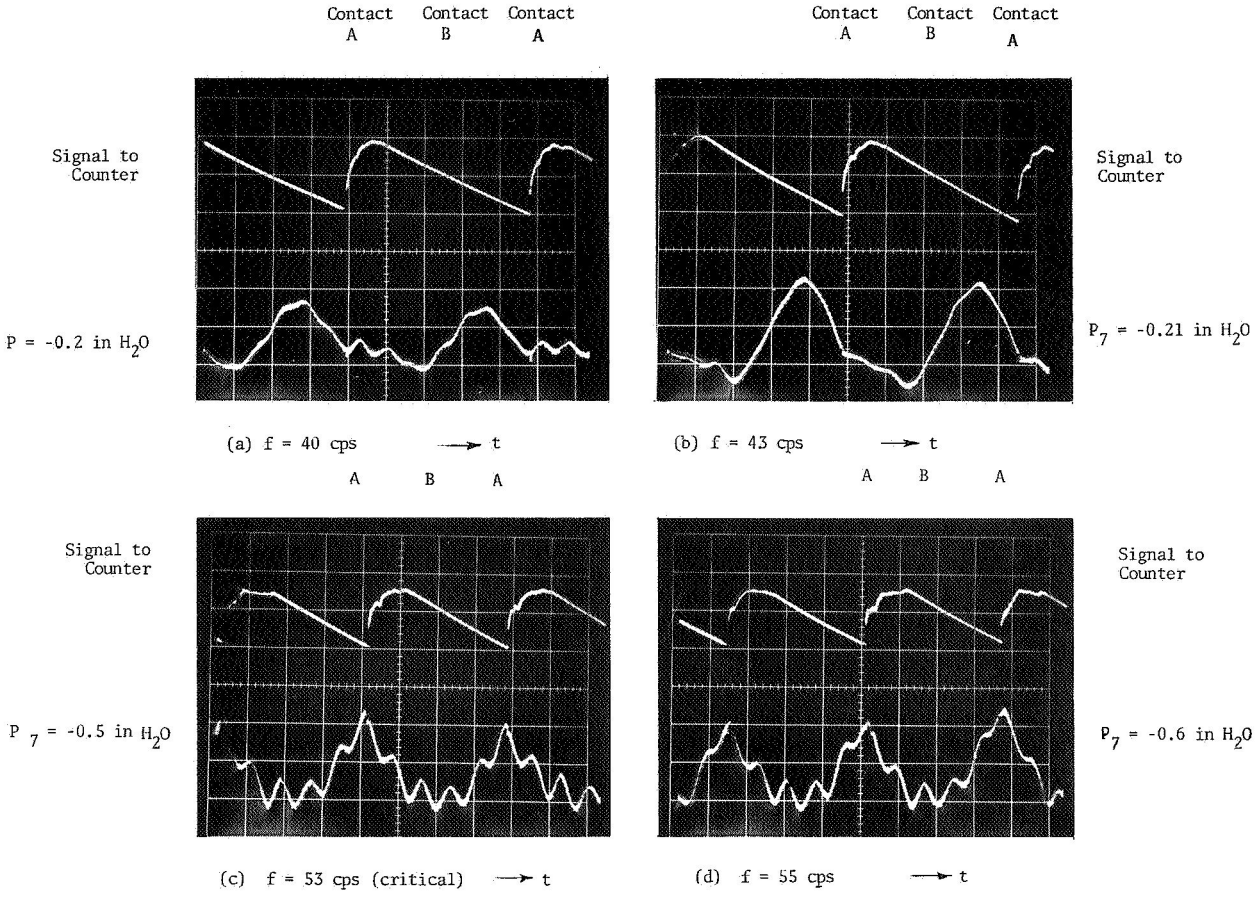

Fig. 8 Photographs Showing Pressure Fluctuation with Respect to Vane Contact Times (Time Scale 5 msec/div Pressure Curves Taken Inversed)

Although the nature of the discontinuity is not known completely, it seems to be a result of complex dynamic resonance between the fluctuating pressure force acting on the vane and the impact force at the instant the oscillating vane hits the contacts. Fig. 8 shows the fluctuating wave forms of the pressure P_7 (tap 7 in Fig. 5) corresponding to the instantaneous contact times of the oscillating vane, where contacts A and B denote the electrically active and electrical inactive contacts respectively (all vertical scales have been taken arbitrarily disregarding the absolute values and the fluctuating pressure curves were taken with inverted signs for convenience). As the flow rate increases, the location of the maximum value of P_7 moves to the right until it reaches the contact A, when the discontinuity (critical frequency) appears. Thereafter, it seems to repeat itself almost periodically. Neither sonic nor choked flow [15] conditions were observed in this work, especially in discontinuity phenomena.

More detailed tests were made as follows to investigate various influences of operating conditions and geometry of the test model.

Influence of Diffuser Angle

Five different diffuser angles from 20° to 60° with increments of 10° were tested, as can be seen from Figs. 9 and 10 in order to investigate the relationships, flow rate vs. frequency and flow rate vs. pressure distribution, with the operating conditions and geometry of P_S= 60 psig, t_ℓ = 74°F, A.R. = 4 and full size ($\ell_1 h_1$ shown in Fig. 11) vane for Case 1, where P_S, t_ℓ and A.R. represent supply pressure to the F-P flowmeter, line temperature and aspect ratio respectively. A decrease in diffuser angle causes the frequency sensitivity to increase and the flow rate at which the first discontinuity appears decreases, in the range of diffuser angles (θ) about 30° to 50° with A.R. = 4 (Fig. 9). The pressure distributions along the inside of the diverging section of the passage during operation are shown to be almost linear and little affected by the change of diffuser angle except P_7(Fig. 10).

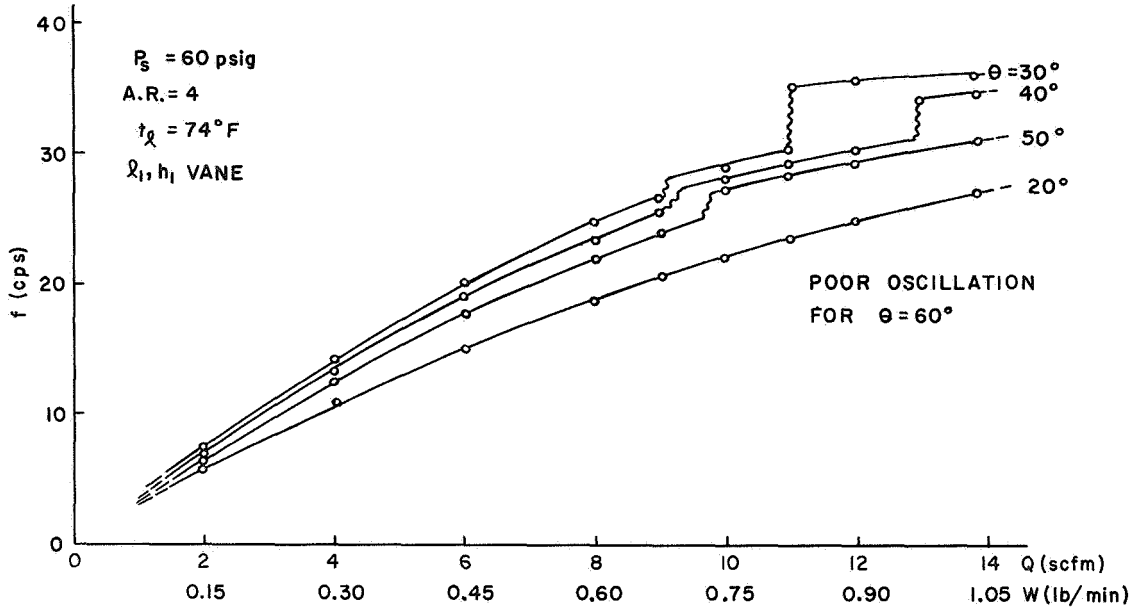

Fig. 9 Influence of Diffuser Angle on Frequency -- Case 1

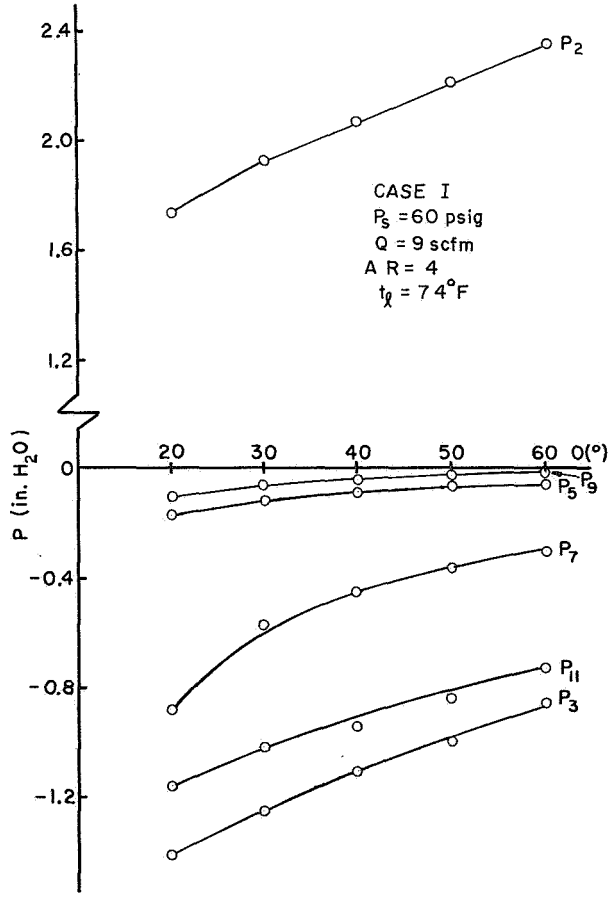

Fig. 10 Influence of Diffuser Angle on Pressure Distribution -- Case I

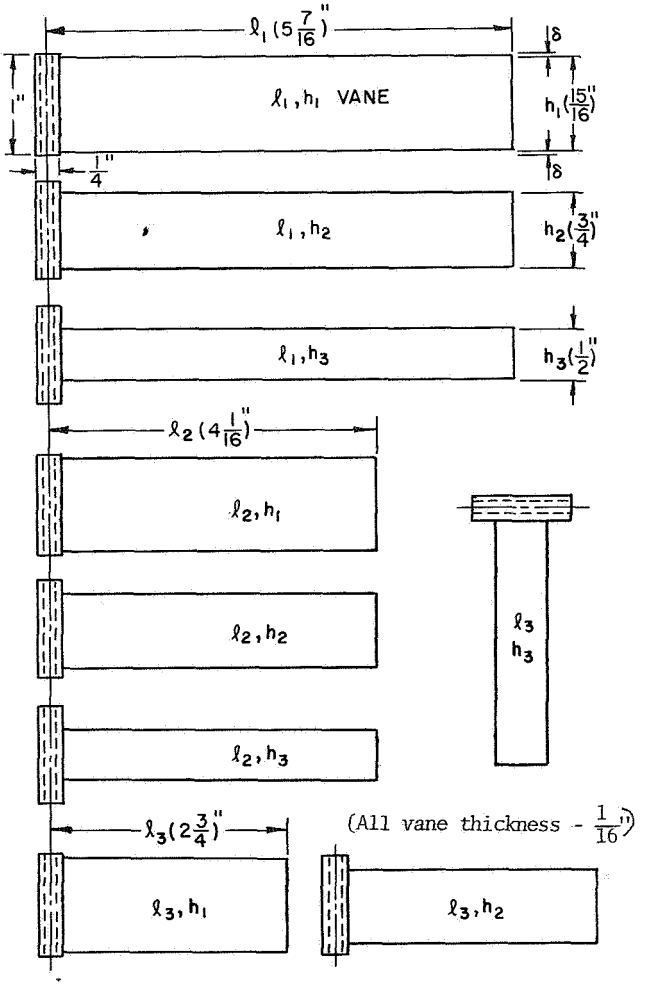

Fig. 11 Nine Models of Oscillating Vane

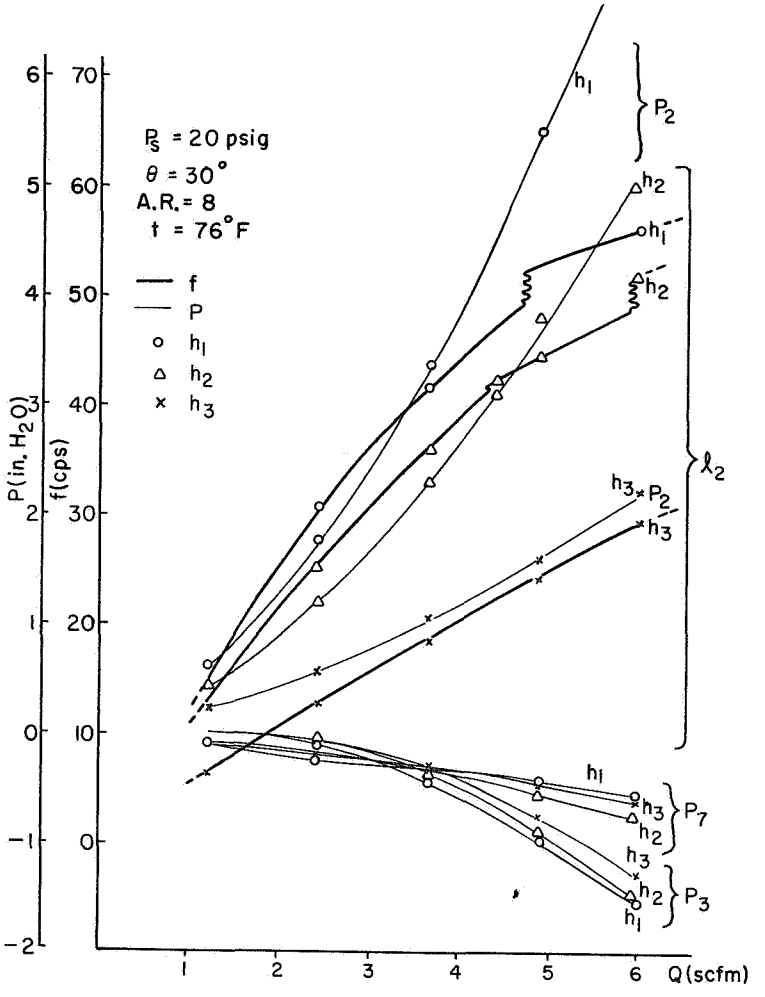

Fig. 12a Influence of Vane Height -- Case I, ℓ_i

Influence of the Length and Height of the Oscillating Vane

Three different lengths and heights, i.e. full, three quarter, and half size respectively, have been chosen and tested in order to investigate the influence of the oscillating vane size on oscillating frequency and pressure distributions, with the operating conditions and geometries of P_s = 20 psig, t_ℓ = 76°F, A.R. = 8 and θ = 30° for Case I. Accordingly, nine different vane models were tested with the results shown in Figs. 12a through 12c, for various combinations of length and height of the vane as shown in Fig. 11 (note that the ideal full height of the vane must be exactly 1 in. but it was reduced to allow clearance δ = 1/32 in. on each side) and the vane thickness is 1/16 in.

A summary of the data obtained from the three length group tests shows, in general, the following characteristics, as shown in Figs. 12a through 12c:

1. The frequency sensitivity generally increases as ℓ decreases and h increases.

2. In general P_2 and P_3 increase and decrease respectively as ℓ or h increases.

Influence of Gas Density

In order to investigate the influence of the fluid density, He (helium) gas was used for about the same operating conditions and geometry of the test model as those in the air tests. A back pressure control box (lucite) was used to prevent the ambient air from contaminating the He around the oscillating vane. Therefore, only density corrections were required for the F-P flowmeter readings and then flow rate vs.

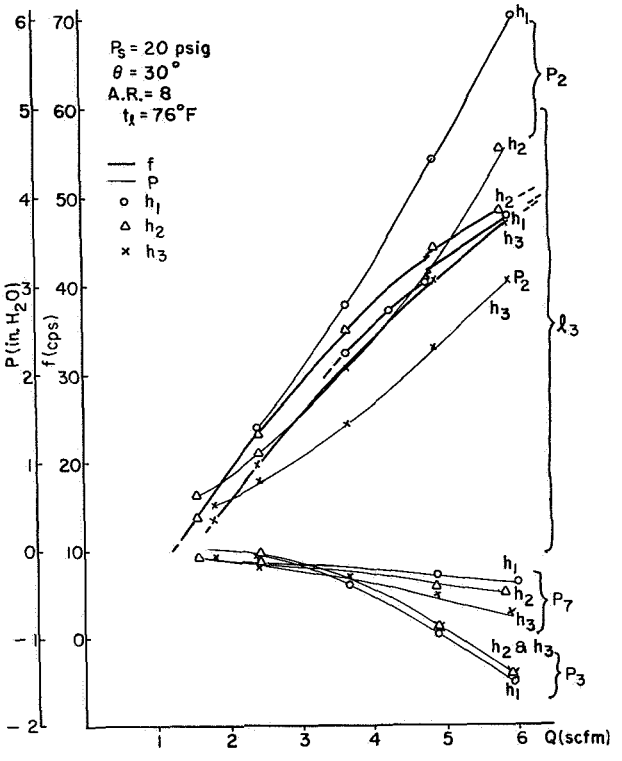

Fig. 12b Influence of Vane Height -- Case I, ℓ_2

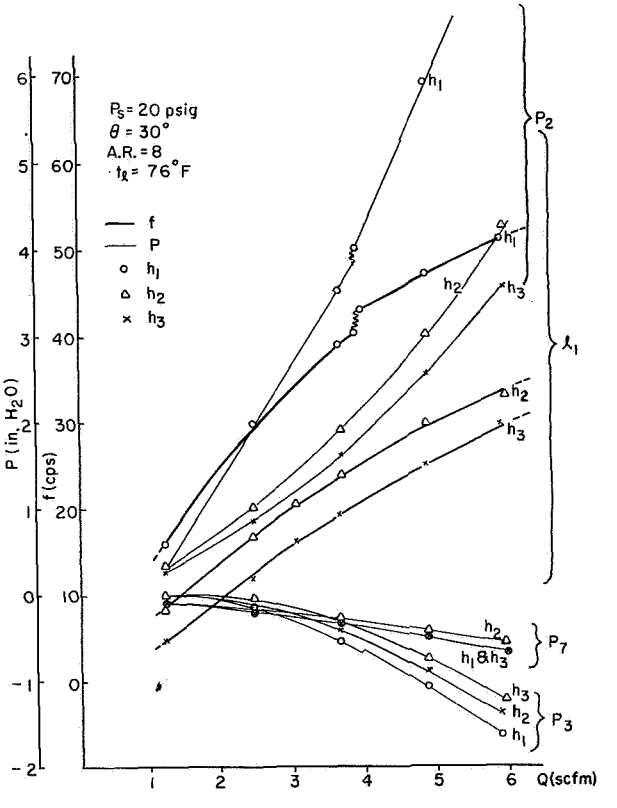

Fig. 12c Influence of Vane Height -- Case I, ℓ_3

frequency curves were plotted, being compared with those from the air tests as shown in Figs. 13a and 13b. The following is the specifications of He used [16].

grade . . . 99.995%

Relative density at STP* . . . 0.137 (air - 1.000)

It should be noted that the density corrections of the F-P readings for He were made in such a way that for volume flow rate;

corrected flow = indicated flow rate x density correction factor and for mass flow rate;

corrected flow = indicated flow rate/density correction factor i.e..

*STP - Standard temperature and pressure (70°F and 14.7 psia)

$$\frac{Q_h}{Q_a} = \frac{\rho_a}{\rho_h} \quad \text{and} \quad \frac{W_h}{W_a} = \frac{\rho_h}{\rho_a}$$

where Q, W, and ρ are volume flow rate, mass flow rate, and fluid density respectively and subscripts a and h denote air and He respectively.

The frequency sensitivity obtained from He tests was, in general, much lower for the same scfm but, on the contrary, much higher for the same mass flow rate than that from the air tests, no matter which cases and vane models had been employed.

As an experiment, it was decided to try and use the same density correction factor technique on the oscillating vane sensor as is used on the Fischer-Porter flowmeter. In Figs. 13a and 13b the curves for air have been "density corrected" for volume flow rate and mass flow rate tests and compared to the actual curves for helium.

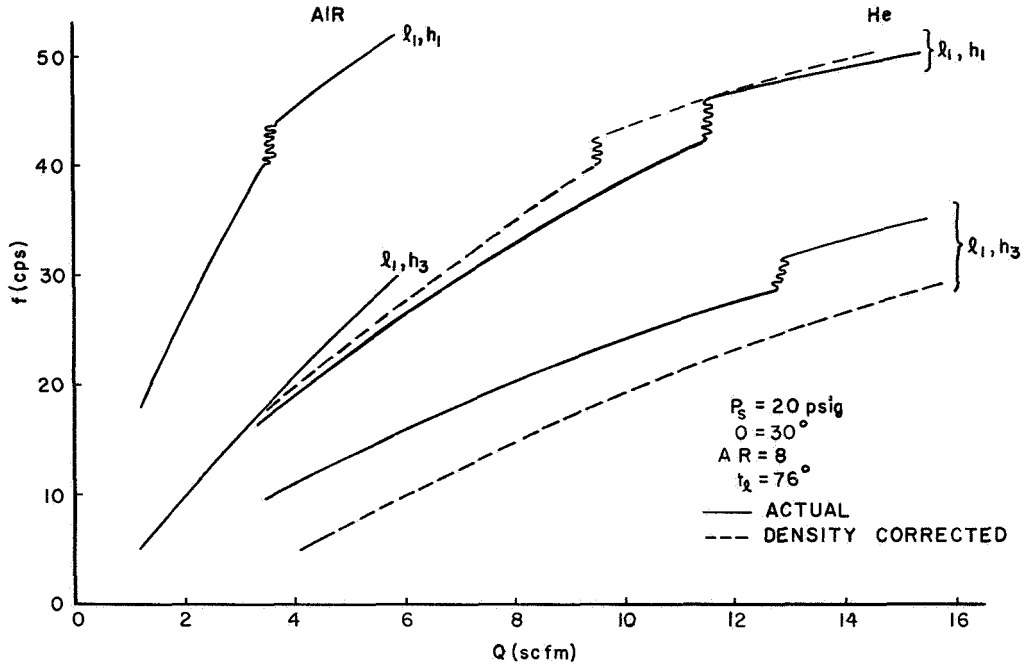

Fig. 13a Influence of Gas Density -- Case I, Q

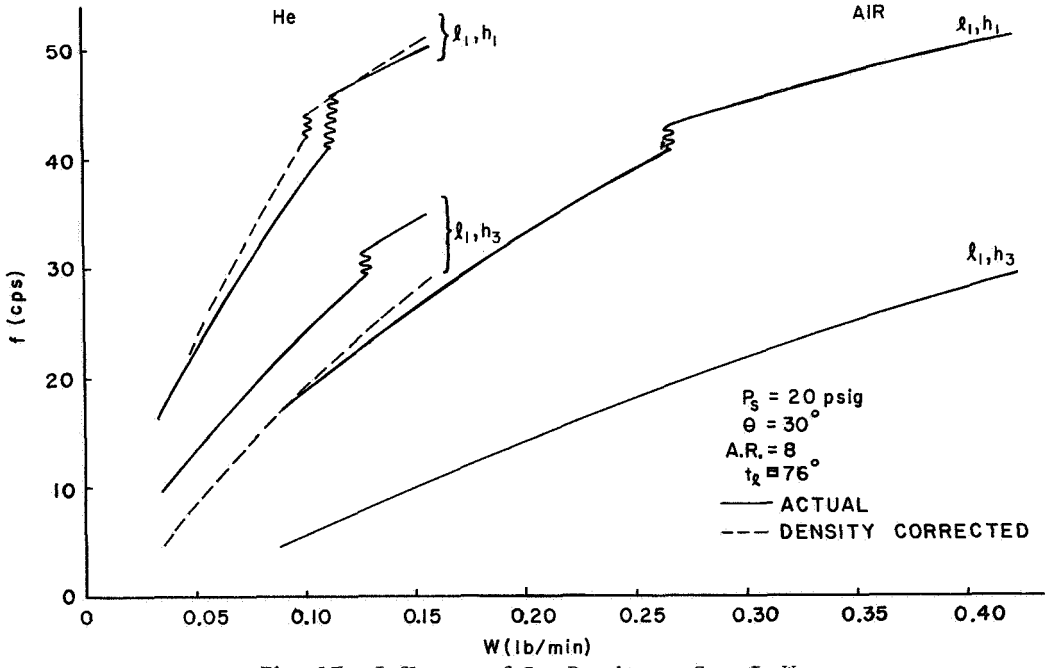

Fig. 13b Influence of Gas Density -- Case I, W

Briefly, the oscillating vane-digital flow rate sensor of this experimental work is based upon a flow rate causing the vane to oscillate and using the frequency of oscillation to indicate rate of flow. It has a good digital output but a special technique is needed to suppress contact noise. The device is capable of indirectly measuring either volume or mass flow rate over a fairly wide, linear range of flow rate at least 13:1 in a few cases. Also, it offers very little obstruction to the flow so that the total pressure drop through the device is less than 2.0 in. H_2O with a flow rate of about 10.0 scfm.

A Masters thesis entitled Experimental Study of an Oscillating Vane-Digital Flow Rate Sensor, by M. B. Song, has been submitted to The Pennsylvania State University Graduate School.

This work was supported in part by NASA Grant NGR 39-009-023.

FLUID JET AMPLIFIER DYNAMICS

A. K. Stiffler, NASA Trainee in M. E.

In the last Research Report [8] some preliminary curves were presented which illustrated the behavior of turbulent jet mean velocity profiles when these jets were perturbed at the nozzle region. These perturbations were directed through one port, maintaining the opposing port pressure constant. A theoretical model is now proposed to predict jet velocity during its dynamic state. With this model in mind, it is desirable to excite both control ports 180° out of phase so that symmetry is assured in the analysis.

A Simple Model of Dynamic Jet Deflection

It has been established that, at least for low frequency and small amplitude disturbances, little if any change occurs in the turbulent mixing of the jet even though a physical deflection of the jet is evident. Thus a simple model, based on the assumption that the control port dynamics merely alter the direction of the jet without changing the effective velocity profile of the jet, seems reasonable. The purpose of this model is to formulate the velocity as a function of time at some stationary point (x_a, y_a). With this model it is only necessary to study motion of the jet centerline. Fig. 14 shows the profile downstream at two instants of time.

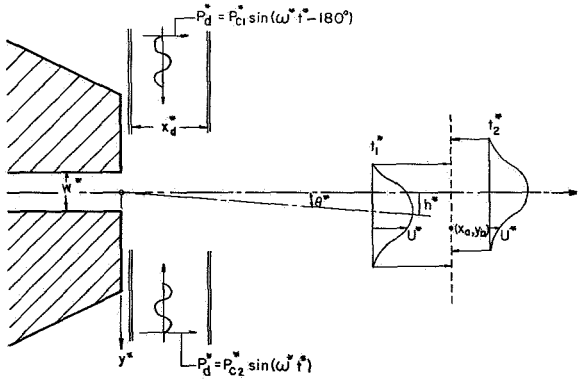

Fig. 14 Representation of Perturbed Mean Velocity Profiles

Control Region: $0 \leq x^* \leq x_d^*$

If the assumption is made that the axial velocity is constant across the jet (equal to U_o), an approach employed by Gurski [17], the momentum equations in a previous report [7] reduce to

$$\frac{\partial V}{\partial t'} + \frac{\partial V}{\partial x} = \frac{1}{2} P_c \sin(\omega t') \qquad (1)$$

where

$$x = \frac{x^*}{w}$$

$$V = \frac{V^*}{U_o}$$

$$t' = \frac{U_o t^*}{w}$$

$$P_c = \frac{P_{c1}^* - P_{c2}^*}{\rho U_o^2}$$

$$\omega = \frac{\omega^* w}{U_o}$$

Variables with an asterisk are the actual variables (i.e. not normalized).

Defining the normalized jet centerline position as $h = h^*/w$, the total derivative of h gives the normalized transverse velocity V of the fluid in the jet.

$$\frac{Dh}{Dt} = \frac{\partial h}{\partial x} + \frac{\partial h}{\partial t'} = V \qquad (2)$$

with boundary conditions

(i) $h(o,t) = \partial h/\partial x\ (x,o) = 0$

(ii) $h(x,o) = \partial h/\partial t'\ (o,t) = 0,$

Equation (1) can be written as

$$\frac{\partial^2 h}{\partial (t')^2} + \frac{\partial^2 h}{\partial x \partial t'} + \frac{\partial^2 h}{\partial x^2} = \frac{1}{2} P_c \sin(\omega t') \qquad (3)$$

with solution in the s domain, based on the Laplace transformation,

$$\int_o^\infty e^{-st'} f(t'),$$

$$H(s) = \frac{\frac{1}{2} P_c \omega}{s^2(s^2+\omega^2)} [1 - e^{sx} - sxe^{-sx}] \qquad (4)$$

The jet position in the time domain at x_d is then obtained by inverse transformation of Eq. (4),

$$h(x_d,t') = h_d = \frac{1}{2} (P_c/\omega^2) \{\sin(\omega t') [\cos \tau_1 + \tau_1 \sin \tau_1 - 1] + \cos(\omega t') [\tau_1 \cos \tau_1 - \sin \tau_1]\} \quad \text{for } t' > x_d \qquad (5)$$

where $\tau_1 = \omega x_d$ (transport delay time). In terms of actual variables

$$\tau_1 = \frac{\omega^* x_d^*}{U_o} \qquad (6)$$

Substitution of $\omega^*/2\pi$=1000 cycles/sec., x_d^* = 1/16 in., U_o^* = 150 ft./sec., results in τ_1 = 0.43. In most applications with fluidic devices τ_1 is much smaller than this value so that the assumption: $\tau_1 << 1$, is generally valid. Thus

$$h_d = \frac{1}{2} P_c (x_d)^2 \left[\frac{1}{2} \sin(\omega t') - \tau_1/3 \cos(\omega t')\right] \quad (7)$$

From Eqs. (2) and (4), the transverse velocity of the jet fluid at x_d is given by

$$V_d = \frac{\partial h}{\partial x}(x_d, t') + \frac{\partial h}{\partial t'}(x_d, t') \quad (8)$$

$$V_d = \frac{1}{2}(P_c/\omega)\{\cos(\omega t')[\cos\tau_1 - 1] + \sin(\omega t')[\sin\tau_1]\}$$

A similar approximation for V_d is then given by

$$V_d = \frac{1}{2} P_c x_d \left[-\tau_1/2 \cos(\omega t') + \sin(\omega t')\right] \quad (9)$$

Jet Displacement Downstream of the Control Port Region

After leaving the control port region, the angle between the jet centerline and the nozzle axis remains the same as at $x = x_d$, namely

$$\tan\Theta = V_d^*/U_o^* = V_d = \text{const.} \quad (10)$$

The displacement h^* at distance x^* downstream from x_d^* can be obtained from

$$\frac{h^* - h_d^*}{x^* - x_d^*} = \tan\Theta$$

or

$$h = V_d(x - x_d) + h_d \quad (11)$$

Using Eqs. (7) and (9) and rearranging,

$$h(t') = \frac{1}{2} P_c x_d (x - x_d/2) \sin[(\omega t') - \tau_2], \quad (12)$$

where

$$\tau_2 = \frac{\tau_1}{2}\left[1 - \frac{0.17}{(2x/x_d) - 1}\right] \simeq \frac{\tau_1}{2}$$

Jet Velocity Downstream

Townsend [18] has shown that mean velocity profiles beyond x = 6 can be described for an undeflected jet by

$$U^*/U_{c\ell} = U_s = f(\eta)$$

where $U_{c\ell}$ is the centerline velocity and $\eta = y/x - x_o$, with x_o constant. There are numerous functional forms for U_s to choose from in the literature. The choice here is the form

$$U_s = e^{-k\eta^2} \quad (13)$$

This form is somewhat different from the form used for the initial mixing layer in [7]. The transport time for a particle to move from x_d^* to x_a^* is described by

$$\tau_t = \int_{x_d^*}^{x_a^*} \frac{dx^*}{U^*} \quad (14)$$

During a sinusoidal disturbance, the jet centerline is displaced according to Eq. (12), and the fluid velocity in the jet will be described by

$$U_s(t', x, y) = e^{-k\left[\frac{y + h(t')}{x - x_o}\right]^2}$$

or

$$U_s(t', \eta) = e^{-k\left[\eta + \frac{h(t')}{x - x_o}\right]^2} \quad (15)$$

Rewriting Eq. (15),

$$U_s(t', \eta) = e^{-k\{\eta + m \sin[(\omega t') - \tau]\}^2} \quad (16)$$

where

$$m = 1/2\, P_c x_d \left(\frac{x - 0.5x_d}{x - x_o}\right), \quad \tau = \tau_2 + \tau_t$$

A series expansion of Eq. (16) is

$$U_s(t', \eta) = U_s(0, \eta) + m \frac{dU_s(0,\eta)}{d\eta} \sin[(\omega t') - \tau] + \frac{m^2}{2!} \frac{d^2 U_s(0,\eta)}{d\eta^2} \sin^2[(\omega t') - \tau] + \ldots \quad (17)$$

Defining $U_p(t', \eta)$ as the difference: $U_s(t', \eta) - U_s(0, \eta)$,

$$U_p(t', \eta) = U_{p1} \sin[(\omega t') - \tau] + U_{p2} \sin^2[(\omega t') - \tau] + \ldots$$

where

$$U_{p1} = -2k\eta m\, U_s(0, \eta)$$

$$U_{p2} = -km^2(1 - 2k\eta^2)\, U_s(0, \eta)$$

$$U_{p3} = 2/3\, k^2 m^3 \eta (3 - 2k\eta^2)\, U_s(0, \eta)$$

$$U_{p4} = 1/6\, k^2 m^4 (3 - 12k\eta^2 + 4k^2\eta^4)\, U_s(0, \eta) .$$

The first four terms on the right reduce to

$$U_p(t', \eta) = 1/2\,[U_{p2} + 3/4\, U_{p4}] + [U_{p1} + 3/4\, U_{p3}] \sin[(\omega t') - \tau] - 1/2\,[U_{p2} + 3/4\, U_{p4}] \cos 2[(\omega t') - \tau] - 1/4\, U_{p3} \sin 3[(\omega t') - \tau] \quad (18)$$

Thus, the dynamic profile can be determined with an anemometer and wave analyzer by successive measurement of amplitude at frequencies n, 2n, 3n . . . . .

This work has been partly supported by NASA Grant NGR 39-009-023.

ANALYSIS OF SIMPLIFIED LINEAR MODEL FOR FLUID TRANSMISSION LINES

R. R. Huber, Research Assistant in M. E.

The collecting of experimental data has been completed, the test apparatus and test procedure being described in SCL Report No. 8 [8]. The task is now to model the line with a simplified mathematical model that agrees reasonably well with the experimental data.

The line is being modeled mathematically as a line with constant, distributed resistance, inertance, and capacitance. The equations describing the fluid pressure and flow are:

$$\frac{\partial P}{\partial x} = -\left(I\frac{\partial P}{\partial t} + RQ\right) \qquad (1)$$

$$\frac{\partial Q}{\partial x} = -C\frac{\partial P}{\partial t} \qquad (2)$$

where

$P(x,t)$ = pressure, lb/in^2

$Q(x,t)$ = volume flow rate, in^3/sec

I = inertance, $lb\text{-}sec^2/in^6$

R = resistance, $lb\text{-}sec/in^6$

C = capacitance, in^4/lb

x = distance along the line, in.

Most of the solutions found in the literature for these equations, or simplifications of these equations, are presented for zero initial conditions. Starting with the solutions in this form, it often becomes difficult to include the effects of non-zero initial conditions. Simplified solutions of the above equations have now been carried out for non-zero initial conditions. The initial conditions are,

$$Q(x,0) = Q_0 \qquad (3)$$

$$\left.\frac{\partial Q(x,t)}{\partial t}\right|_{\substack{x=x\\t=0}} = 0 \qquad (4)$$

$$P(x,0) = P_0 - Q_0 R x \qquad (5)$$

$$\left.\frac{\partial P(x,t)}{\partial t}\right|_{\substack{x=x\\t=0}} = 0 \qquad (6)$$

where

P_0 = constant tank pressure

Q_0 = initially constant steady flow rate

which are for a line with an initial constant flow rate resulting in a uniform pressure drop per unit length of line. The boundary conditions are,

$$P(0,t) = P_a(t) \qquad (7)$$

$$Q(L,t) = Q_b(t) \qquad (8)$$

where L = length of the line.

Laplace transforming Eqs. (1) and (2) utilizing the initial conditions in the transformation and the boundary conditions to evaluate the constants, results in the following pair of transformed equations:

$$\mathbf{Q}_a(s) = \frac{1}{\cosh\gamma L}\left[\left(\mathbf{Q}_b - \frac{Q_o}{s}\right) + \frac{Cs}{\gamma}\left(\mathbf{P}_a - \frac{P_o}{s}\right)\sinh\gamma L\right] + \frac{Q_o}{s} \qquad (9)$$

$$\mathbf{P}_b(s) = \left[-\left(\frac{Is+R}{\gamma}\right)\left(\mathbf{Q}_b - \frac{Q_o}{s}\right) - \left(\mathbf{P}_a - \frac{P_o}{s}\right)\sinh\gamma L\right]\tanh\gamma L + \left(\mathbf{P}_a - \frac{P_o}{s}\right)\cosh\gamma L + \frac{P_o - Q_o RL}{s} \qquad (10)$$

where $\gamma = \sqrt{ICs^2 + RCs}$.

Specific solutions will now be given for boundary conditions corresponding to the experimental test conditions; that is,

$$P(0,t) = P_0 \qquad (11)$$

$$Q(L,t) = 0,\ t > 0 \qquad (12)$$

For the frictionless case ($R = 0$), the solutions of Eqs. (9) and (10) are:

$$Q_a(t) = Q_0 - 2Q_0\left[U_s(t-T_e) - U_s(t-3T_e) + U_s(t-5T_e) - U_s(t-7T_e) + \ldots\right] \qquad (13)$$

$$P_b(t) = P_0 + Z_c Q_0 - 2Z_c Q_0\left[U_s(t-2T_e) - U_s(t-4T_e) + U_s(t-6T_e) - U_s(t-8T_e) + \ldots\right] \qquad (14)$$

where $U_s(t-b) = 0,\ t < b$; $= 1,\ t > b$ } unit step function

Z_c = characteristic impedance of the line, $\sqrt{I/C}$

T_e = wave propagation time for distance L

It should be noted that these solutions were obtained directly without having to shift the time in the equations to obtain a set of physically realizable equations.

The following solution includes the effects of resistance. The propagation constant γ and the characteristic impedance Z_c will be simplified as in

an unpublished set of notes by Reid [19]. The validity of this simplification for transient response is questionable. The propagation constant and the characteristic impedance become,

$$\gamma L \approx - \alpha + T_e s \tag{15}$$

$$Z_c = \sqrt{I/C} \tag{16}$$

where $\alpha = \frac{-RL}{2} \sqrt{\frac{C}{I}}$.

The final solutions resulting from the use of these simplifications are:

$$Q_a(t) = Q_0 - 2Q_0 \left[e^{\alpha} U_s(t-T_e) - e^{3\alpha} U_s(t-3T_e) + e^{5\alpha} U_s(t-5T_e) - e^{7\alpha} U_s(t-7T_e) + \ldots\right] \tag{17}$$

$$P_b(b) = (P_0 - Q_0 RL) + Z_c Q_0 - 2Z_c Q_0 \left[e^{2\alpha} U_s(t-2T_e) - e^{4\alpha} U_s(t-4T_e) + e^{6\alpha} U_s(t-6T_e) - e^{8\alpha} U_s(t-8T_e) + \ldots\right] \tag{18}$$

Further work is planned to obtain the complete solution of the RIC model with no simplifications. If possible, simplifications will then be made in order to obtain a reasonably simpled model of the line.

This research is supported by NASA Grant NGR 39-009-023.

FLUID LINE DYNAMICS

R. G. Leonard, Instructor in M. E.

In order to further the understanding of the dynamic performance of fluid filled transmission lines, a Ph.D. thesis research program is now under way. This work, which deals primarily with liquid filled lines, is a continuation of previous SCL activities in this area which have been reported earlier [4, 5, 6, 7, 8]. This study is focused on the development of a simplified mathematical model which will adequately describe the characteristics of a fluid filled line which might be part of a fluid system.

The experimental phase of this study is concerned with the nature of the fluid flow under conditions of water hammer. To facilitate this study a test section, shown in Fig. 15, has been designed and installed in the test line as shown in Fig. 16. The test section was fabricated of clear plastic to allow visual observation of the flow. A method of flow visualization known as the Hydrogen Bubble Technique was chosen for this study. This technique is convenient in that if offers a minimum obstruction to the flow (as compared with other velocity measuring instruments). With the aid of photography a large portion of the flow field can be examined in a single "measurement".

The valve included in the test section was designed to provide the rapid closure required to study the water hammer phenomena. A pneumatic ram is used to position the valve in order to realize the short closing times.

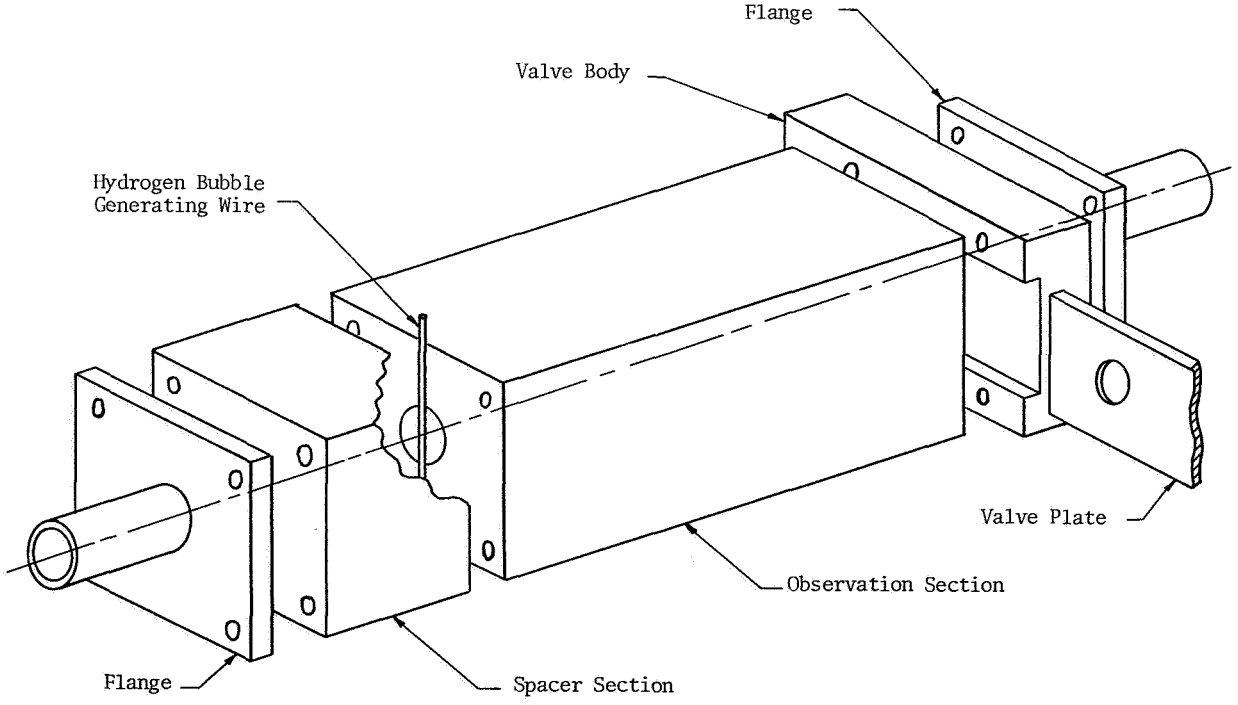

Fig. 15 Exploded View of Test Section

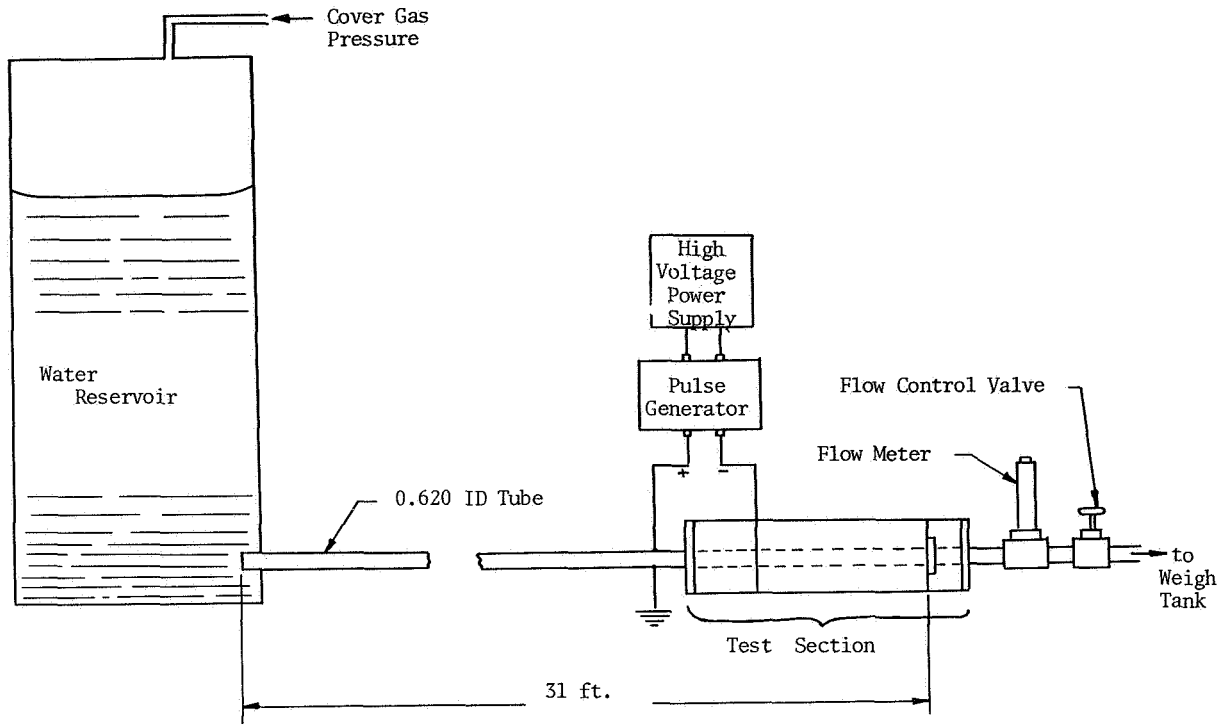

Fig. 16 Overall Arrangement of Test Apparatus

Some preliminary tests with the hydrogen bubble generator were conducted using a one-inch clear plastic tube mounted on a small water table. For these tests a wire was strung horizontally across a diameter of the tube and a brass liner was inserted into the tube upstream to serve as the other electrode. When a negative potential is applied to the wire, tiny bubbles of hydrogen are formed on the surface of the wire and are swept downstream from the wire as soon as they grow to a critical size. Several different wire sizes were tried, from 0.010 to 0.001 in. diameter, and it was concluded that the smaller size wire was necessary in order to obtain small bubbles which would not rise rapidly due to the bouyant force. Davis and Fox [20] determined that the diameter of the bubbles formed is approximately the same as the diameter of the generating wire. The smaller bubbles also attain the velocity of the surrounding fluid more quickly than do the large bubbles. These tests also indicated that it was necessary to separate the two electrodes by at least one tube diameter so as to achieve a relatively uniform electric field and thus obtain more uniform bubble generation. A certain period of "aging" was required (several minutes) before a given wire would generate bubbles uniformly, and then after a period of time, (an hour or so of operation) the quality of the generation would deteriorate. For certain materials which could withstand the oxidizing caused by the generation of oxygen at the wire, a brief period of operation with the polarity reversed tended to restore the wire and result in the production of good quality hydrogen bubbles with normal polarity. The water table tests were conducted with voltage levels ranging from 50 to 400 volts and it was found that the optimum voltage level varied with the electrode spacing and the fluid velocity.

The voltage potential is applied to the wire by an electronic multi-vibrator circuit which was designed to provide the wire with high voltage pulses of variable pulse length and pulse spacing.

Initial attempts to carry out digital computer solutions of approximations to the Navier-Stokes equations have been started, based on a multi-lumped model of the complete length of line.

This work has been supported by a special grant-in-aid from the Rockwell Manufacturing Co.

OPTIMIZER RESEARCH

R. W. Mayne, Graduate Fellow in M. E.

In earlier SCL Reports [7,8] work in this general area was discussed under the title "Electrohydraulic Optimizer" and was devoted primarily to the use of electronic and hydraulic components in realizing a prime mover optimization scheme proposed by Schweitzer et. al. [21]. The basic features of this scheme are the control of the prime mover output power level by a primary input variable (e.g. throttle setting) and the optimization of an auxiliary variable (e.g. spark timing) to

maximize the output power at a given setting of the primary input. The actual optimization process is implemented by an extremum control system sensing angular acceleration of the prime mover output shaft and using this acceleration signal to seek the optimum value of the auxiliary variable. Continuing research in this general area has two aims: first, to investigate and compare the relatively simple extremum control systems which could be used in this application and second, to provide a fluidic realization of the extremum controller or optimizer. It is the purpose of this report to briefly discuss the extremum control techniques under consideration.

The extremum controllers most suited for general application to prime mover systems should be relatively simple in nature, requiring a minimum of logic and memory. Of particular interest are variations of the divider-optimizer discussed by Frait and Eckman [22] and the external perturbation system which was investigated by Eveleigh [23]. A fluidic logic optimizer developed by Lehtinen and Orner [24] employs still another approach which may also merit attention.

Fig. 17 shows a block diagram of the divider-optimizer as it might be applied to a simplified prime mover system. The quantity T_m is the maximum indicated torque available from the prime mover for a given set of operating conditions and is adjusted here by a single primary system input (e.g. throttle setting), x is the auxiliary variable (e.g. spark timing) upon which the indicated torque (T_i) is also dependent, and x_o is its optimum value. The transfer function G represents the dynamics of the prime mover system, Ω is the angular velocity of the output shaft and α is its angular acceleration. The transfer function Geff represents an approximate dynamic model of G, but with unity gain. External load effects and high frequency internally generated perturbations in the indicated torque due, for example, to the firing of individual engine cylinders have not been shown here. Sensor noise encountered in measuring the angular acceleration of the output shaft has also been excluded. These disturbances may be significant factors and have been deleted only to simplify discussion of the controller operation. The divider-optimizer adjusts the variable x at a rate given by

$$\dot{x} = K\frac{\alpha}{\dot{x}^*} = K\frac{d\Omega}{dx}^*$$

Note that $d\Omega/dx^*$ is an approximation to k dT_i/dx where k is the DC gain of G (hint: start at α and $\dot{x}^*$ respectively and work back to T_i and x respectively). Thus this scheme gives a correction rate which is approximately

$$\dot{x} = kK\frac{dT_i}{dx}$$

This correction rate is proportional to the distance from optimum and at optimum the rate tends to zero, minimizing hunting loss. It is also possible to approximate this proportional action without using an actual divider. Frait and Eckman suggest replacing the divider by a logic circuit and a function generator such that the correction rate is

$$\dot{x} = K(\operatorname{sgn}\frac{\alpha}{\dot{x}^*})\sqrt{|\alpha|}$$

which is equivalent to

$$\dot{x} = K^2(\operatorname{sgn}\frac{\alpha}{\dot{x}^*})\left|\frac{\alpha}{\dot{x}}\right|$$

This correction rate will also approach zero in the steady state and the controller action might be considered pseudo-proportional. This optimizer can be simplified by operation in bang-bang fashion. In this situation $\dot{x}$ would be constant in magnitude with its sign controlled by a logic operation such that

$$\dot{x} = K \operatorname{sgn}(\frac{\alpha}{\dot{x}^*}).$$

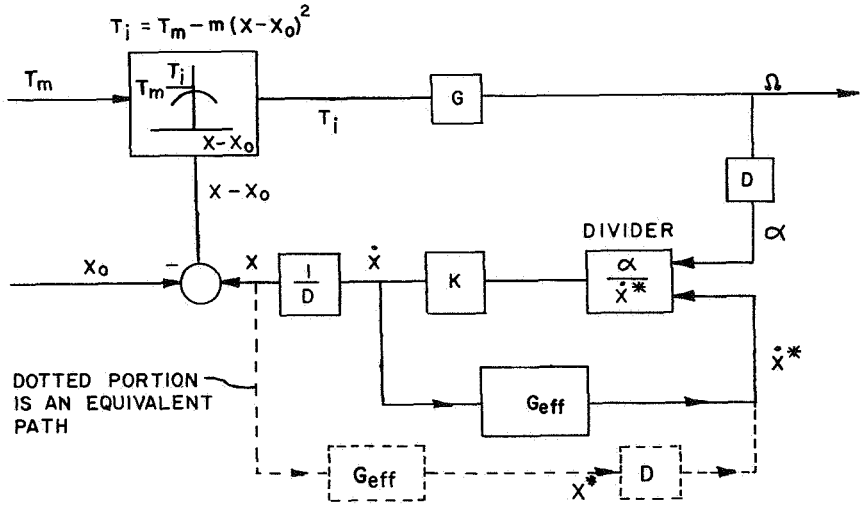

Fig. 17 The Divider Optimizer

There is another type of extremum controller which operates in a manner similar to the bang-bang controller just described. This optimizer has been applied by Lehtinen and Orner [24] and its control law is as below with the magnitude of $\dot{x}$ constant:

1) If α changes from positive to negative, change the sign of $\dot{x}$.

2) If α changes from negative to positive or if α remains positive, do not switch $\dot{x}$.

3) If α remains negative longer than a time T_f, switch $\dot{x}$ at $t = nT_f$ $(n = 1, 2...)$.

This controller requires more complex logic than the bang-bang version of the divider optimizer but a representation of the system dynamics like G_{eff} is not necessary.

We will now consider the extremum control system shown in Fig. 18 which is driven by external perturbations. Basically, this controller compares the phasing of the output signal perturbations with respect to the input signal perturbations suitably filtered (G_{F3}). From this comparison the proper $\dot{x}$ signal is obtained to drive x toward x_o. To more readily understand the controller operation, consider the expression for indicated torque linearized about some operating point x_1:

$$T_i(x_1+\Delta x-x_o) = T_i(x_1-x_o) - 2m(x_1-x_o)\ (\Delta x)$$

or, substituting the perturbation signal for Δx

$$T_i(t) = T_i(x_1-x_o) - 2m(x_1-x_o)\ A \sin \omega_p t$$

The linear transfer function GDG_{F1} is determined so that only frequencies near the perturbation frequency are passed. Thus

$$\alpha_F = -2m(x_1-x_o)\ AB \sin(\omega_p t+\Theta)$$

where B and Θ are the attenuation and phase shift due to GDG_{F1}. The function generator FG has output

$$y = [\mathrm{sgn}\ (\alpha_f \Delta x_f)]\ \left|\alpha_f\right|$$

and the filter G_{F3} has attenuation C and the dynamics of GDG_{F1} so

$$y = \{\mathrm{sgn}\ [-2m(x_1-x_o)\ A^2BC\sin^2(\omega_p t+\Theta)]\}$$

$$\cdot\ \left|-2m(x_1-x_o)\ AB \sin(\omega_p t+\Theta)\right|$$

or

$$y = -2ABm\ [\mathrm{sgn}(x_1-x_o)]\ \left|(x_1-x_o)\sin(\omega_p t+\Theta)\right|$$

With G_{F2} low pass only the time average value is passed giving

$$\dot{x} = -KmAB\ \frac{4}{\pi}\ [\mathrm{sgn}\ (x_1-x_o)]\ \left|(x_1-x_o)\right|$$

and

$$\dot{x} = -KmAB\ \frac{4}{\pi}\ (x_1-x_o)$$

This optimizer therefore has a correction rate proportional to the distance from optimum. However, just as the divider-optimizer, it can also be operated in bang-bang fashion where the logic supplies only the proper sign for $\dot{x}$ (i.e. $y = \mathrm{sgn}\ [\alpha_f \Delta x_f]$). The previous work [7,8] has emphasized this bang-bang perturbation system with the additional restriction that G_{F1} is unity or at most low pass. This system sacrifices efficiency for ease of implementation but may be the most practical for actual operation.

The preceeding material has summarized the extremum control systems which seem most applicable to prime mover optimization using an acceleration signal. The configurations of the divider-optimizer and the external perturbation optimizer have been shown and their use as proportional or bang-bang controllers has been described. Additionally, the controller applied in [21] has also been mentioned. These controllers

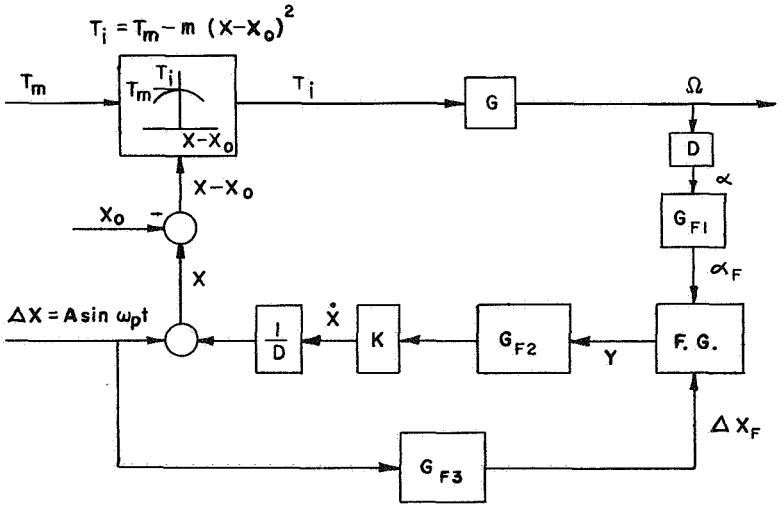

Fig. 18 External Perturbation Extremum Controller

are relatively simple and can be realized without requiring actual division or multiplication. A comparison of their performance in an analog simulation is now in preparation. This comparison will emphasize controller efficiency in terms of response time to changes in x_o for a given hunting loss, sensitivity to torque and accelerometer noise and performance in the face of load and speed changes. Of further interest will be the effect of high frequency noise filters on optimizer performance and sensitivity to simulation of the plant dynamics in the feedback loop.

This work has been supported in part by an NDEA Fellowship and a Grant-in-Aid from the Optimizer Control Corporation.

HELMHOLTZ RESONATOR RESPONSE WITH FM PRESSURE SIGNALS

A. J. Healey, Assistant Professor of M. E.

This work has progressed with studies of the effect of variable frequency pressure inputs to a Helmholtz resontator. The resonator is one type of fluid network which is used in demodulating FM signals which occur naturally in a number of fluidic sensors.

The analysis of the resonator response to variable frequency pressure signals is complicated. Generally speaking, when the frequency (instantaneous frequency) of the input varies, the resonator response can be measured in terms of either the instantaneous frequency of the output or the instantaneous phase difference between input and output, or the instantaneous amplitude of the output signal. Because of the increasing use of phase discrimination as a means for detection of the modulating signal, it was decided that the instantaneous phase difference between input and output and also the instantaneous output frequency would be the output variables of primary interest.

If $\theta(t)$ is the phase shift between input and output signal and Ω_i is the instantaneous input frequency then,

$$\Omega_i = \omega_c + \Delta\omega_i \sin \omega_m t$$

and we can approximate $\theta(t)$ as,

$$\theta(t) = \theta(\omega_c) + \Delta\theta \sin (\omega_m t + \phi_\theta)$$

where $\theta(\omega_c)$ is the phase difference at the carrier frequency ω_c and $\Delta\theta$ is the amplitude of the dynamic phase excursion, ω_m is the modulating frequency and ϕ_θ is the phase shift between the instantaneous input frequency variations and the instantaneous excursions in θ.

The instantaneous output frequency can be written approximately as

$$\Omega_o = \omega_c + \Delta\omega_o \sin (\omega_m t + \phi_\omega)$$

where $\Delta\omega_o$ is the amplitude of the output frequency variations and ϕ_ω is the phase shift between instantaneous output and input frequencies. The problem tackled has been to relate

$$\frac{\Delta\omega_o}{\Delta\omega_i}, \frac{\Delta\theta}{\Delta\omega_i}, \phi_\theta \text{ and } \phi_\omega \text{ to } \omega_m \text{ with } \Delta\omega_i \text{ held constant.}$$

Analytical techniques for predicting the response of these quantities were investigated [25,26,27,28]. Boothe, Ringwall and Kelley [28] showed that some measure of agreement could be obtained for the response, in effect, of $\Delta\theta/\Delta\omega_i$ and ϕ_θ versus ω_m if the low pass equivalent transfer function is used assuming that the modulation index of the FM input signal $\Delta\omega/\omega_m \ll \pi/2$ (i.e. the FM pressure signal) can be approximated by an AM pressure signal [29].

In this project the theoretical results were obtained by numerical solution of the differential equation of the resonator. A sub-routine was developed which then used the time varying output and input signals to calculate instantaneous values for $\Omega_i(t)$, $\theta(t)$ and $\Omega_o(t)$. This program was based on the assumption that the input and output frequencies could be considered constant over one half of a carrier cycle. The base time for each half carrier cycle then determined the instantaneous frequency which was assigned to a time occurring at the middle of that time interval. Instantaneous phase difference between input and output were calculated using successive time intervals denoted by θ in Fig. 19 and assigned to a time at the center of the time interval.

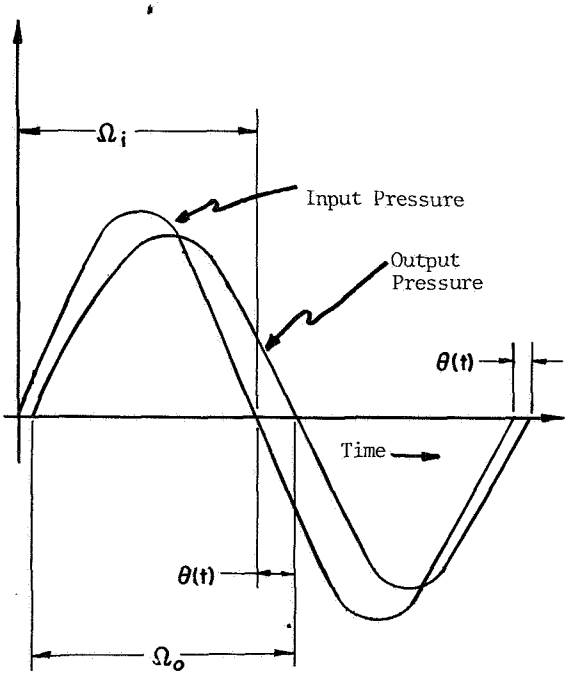

Fig. 19 Diagram Showing Time Intervals Used to Compute $\Omega_i(t)$, $\Omega_o(t)$, $\theta(t)$

Experimental results have been obtained using a wobble plate device with sinusoidally varying speed to obtain the FM input pressure. Analysis of experimental input and output waveforms in the same way as just described for the computed waveforms have resulted in Figs. 20, 21, 22, and 23. Correlation can be seen to be good over a wide range of ω_m. Results obtained using the Boothe, Ringwall and Kelley low pass equivalent transfer function are also shown for comparison indicating generally better agreement for higher values of ω_m where the modulation index $\Delta\omega_i/\omega_m$ is low but poor agreement for intermediate modulating frequencies ($\Delta\omega_i/\omega_m$ about 2) when the low pass equivalent transfer function can no longer be used. Strangely, the low pass equivalent transfer function predicts both ϕ_θ and ϕ_ω well.

This work is the subject of a Masters Thesis which is in preparation by D. W. Fowler. Support was derived in part from the Ford Foundation and also from NASA Grant NGR 39-009-023.

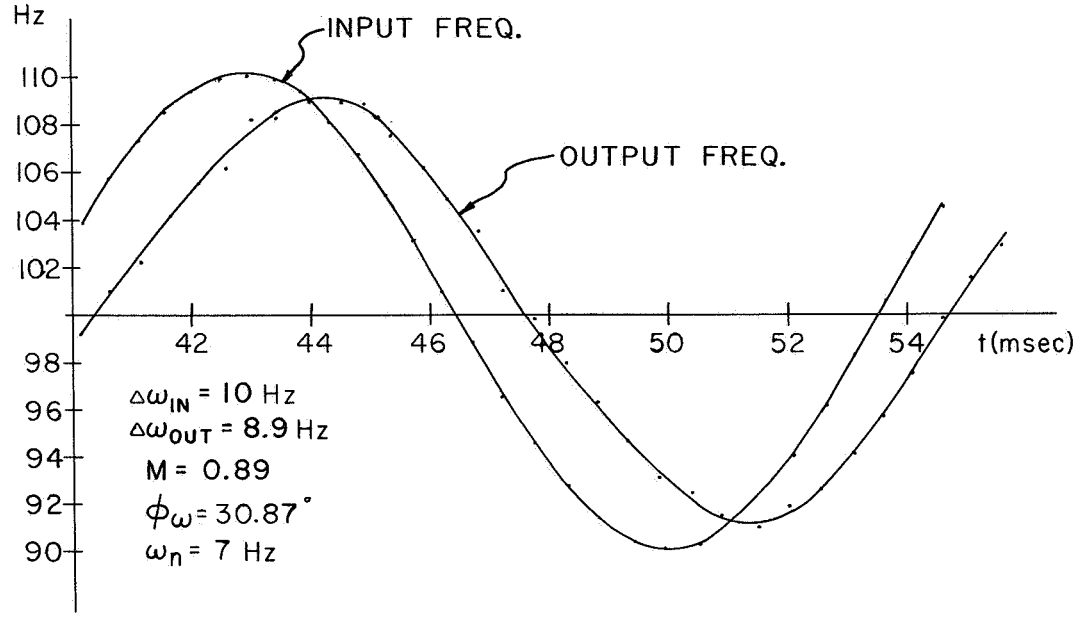

Fig. 20 Computed Values of $\Omega_i(t)$ and $\Omega_o(t)$ Versus Time

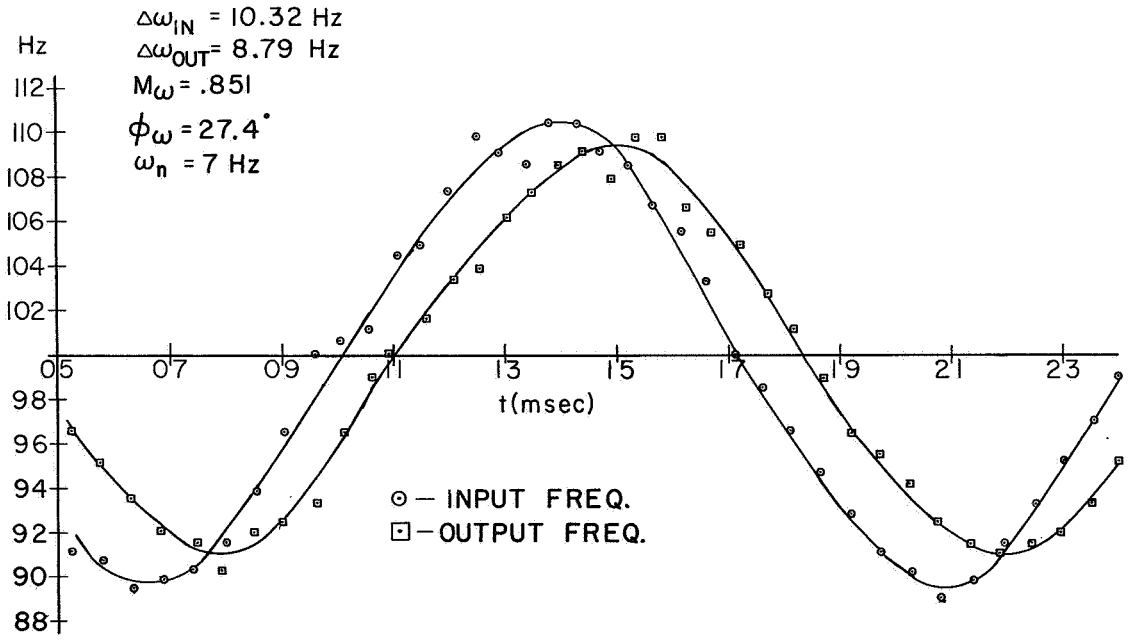

Fig. 21 Experimental Values of $\Omega_i(t)$ and $\Omega_o(t)$ Versus Time

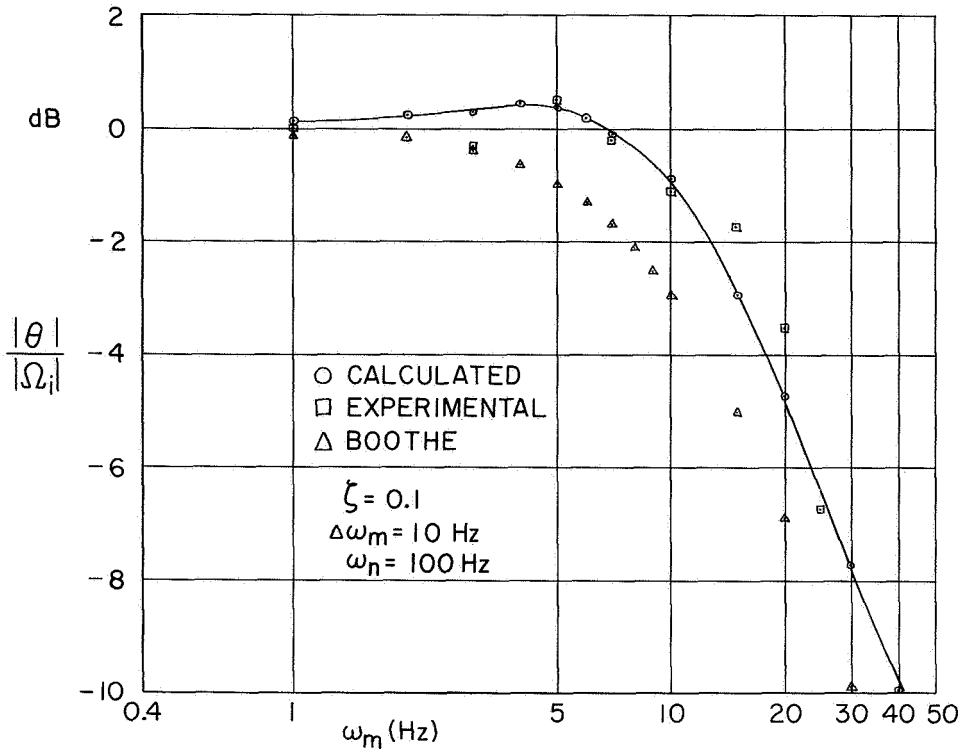

Fig. 22 Amplitude Ratio Response of the Phase Difference Versus Modulating Frequency

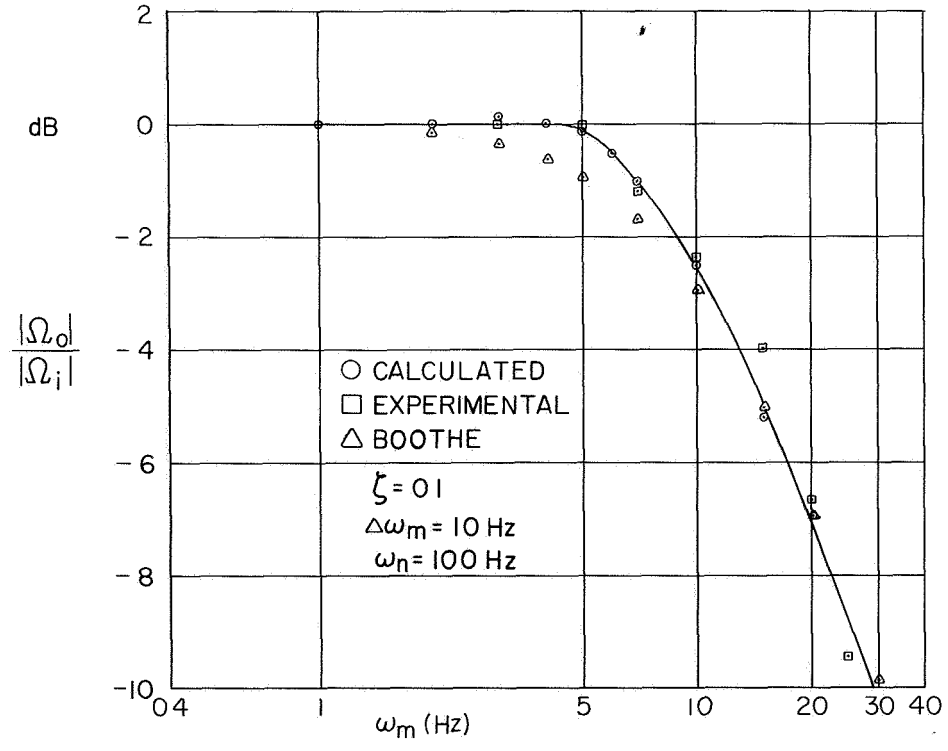

Fig. 23 Amplitude Ratio Response of the Output Frequency Versus Modulating Frequency

ANALOG AMPLIFIER DYNAMIC RESPONSE USING HYDRAULIC OIL

A. J. Healey, Assistant Professor in M. E.

The planned measurement of oil flow rates through the side vents of the amplifier described in the previous report [8] have been made. Taken for a range of control pressure differences, these measurements have shown that the flow component Q_m is essentially of the parabolic form proposed in an earlier publication [30].

Experiments have shown that the flow component Q_m does not change much in magnitude when load resistances are connected to the output ports of the amplifier (equal resistances on each output). Whether or not the functional form of Q_m changes with load resistance under a wide range of conditions is still not really certain.

The measured values for Q_m will be used in the modeling of the dynamic response of the analog amplifier for a range of load impedances. The theoretical model to be used has been described before [30] and extended to include both a flow component across the amplifier receivers and dynamic lags in the power jet deflection*.

This new model is interesting in that the flow component across the receivers has been shown to predict -- at least qualitatively -- the observed experience that as the load impedance increases the amplifier becomes less stable.

This project has been the subject of an M. S. Thesis investigation by K. W. Landsburg which is almost complete.

This has been supported in part by NASA Grant No. NGR 39-009-023.

HYDRAULIC STEPPING MOTOR

I. J. Obradovic, Visiting Professor in M. E.
(NSF Senior Foreign Scientist)

The basic concept for this stepping motor is a fluid motor of the lobed-impeller type, shown schematically in Fig. 24. It has two impellers which rotate in opposite directions. The rotation is assured by a separate gear system on the same shafts with ratio 1:1.

Instead of using passages entering radially as is usual for this type of hydraulic motor, the fluid is introduced and drained axially through the front plate. The four passages a+, a-, b+, b- are shown in Fig. 24. The passages are so arranged that they are alternately opened and closed two at a time by their corresponding impellers. Therefore, each pair of passages serves to drive its corresponding rotor only up to the point where the rotor closes both passages. The direction of rotation depends on which

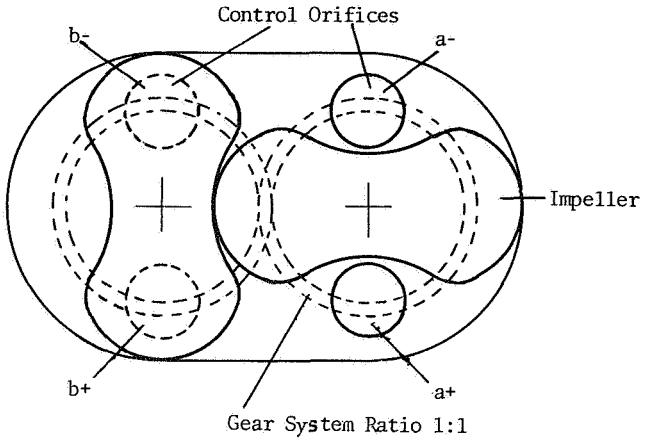

Fig. 24 Lobed Type Impeller Design

one of a given pair is for the supply flow (the other being for exhaust flow). Thus, the motor output shaft normally is advanced by 90° increments each time a new set of passages is connected to supply and exhaust. Thus, a change in flow passage is required for each new increment, and the direction is determined by the polarity applied to a given pair of passages.

An experimental motor has been designed and built, and limited tests have been made on it.

In order to permit remote operation with pulse signals through a single line, a special two spool transfer valve has been designed and built incorporating two small fluid capacitors as shown in Fig. 25. With this scheme of operation, a mean pressure is maintained in the line and positive and negative pulses are transmitted above and below this mean pressure level.

During the pulse interval the stepping motor makes a 90° step and at the same time stores the fluid energy required for an additional 90° step which is made automatically in the same direction during the pulse pause. In this way a nearly continuous motor rotation could be realized.

The piston positions shown in Fig. 25 are for the state in which the fluid pressure in the supply line is at the mean value. The mean positions of pistons A and B vary directly with the mean line pressure. When a positive pulse is transmitted through the input signal line, both pistons move downward, but whereas piston A immediately returns to its mean position when the pressure returns to its mean value, piston B stays down for at least one additional pulse-width-time-interval (due to connection with capacitor 2). Passages 2+ and 2- are never covered by the impellers. In this case the fluid capacitor 2 is connected to 2+ and impeller outflow is controlled by orifices a+ and b+. (Flows are through 2-, a-, and b- for the other direction initiated by a negative pulse.)

The three flexible plate check valves have medium leakage performance but very fast response. They are needed only for temporary action -- the spool valves always provide positive closure in the end.

* In a paper given at the Symposium on Fluidics and Related Internal Flows held on October 22-23, 1968 at The Pennsylvania State University, the proceedings of which are in preparation [31].

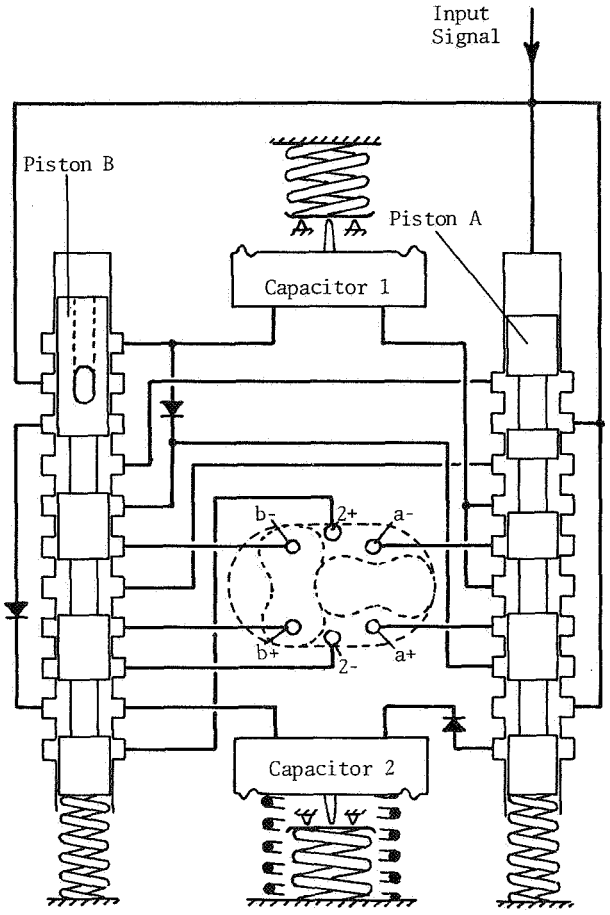

Fig. 25 Schematic Diagram of Transfer Valve

The characteristics required of fluid capacitors 1 and 2 are given in Fig. 26. The pressure discontinuity characteristics separates the two distinct energy storage functions to be carried out by each unit.

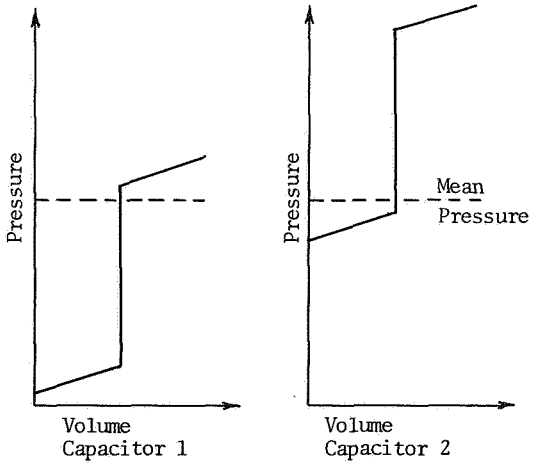

Fig. 26 Pressure-Volume Characteristics of Capacitors 1 and 2

With this motor, valve, and capacitor system it is possible to operate with a hermetically sealed system employing only one fluid line to carry both information and power. Further, the mean flow to the system over a long period of time is essentially zero.

This work has been partly supported by NASA Grant NGR 39-009-023.

THE CONTROL AREA AS A BASIS FOR SELF ADAPTIVE OPTIMAL CONTROL

I. J. Obradovic, Visiting Professor in M. E.
(NSF Senior Foreign Scientist)

The control area was probably applied for the first time in 1940 in the author's Doctoral thesis for evaluating a controller constant in a feedback system subjected to step inputs. In a paper published by the author two years later [32], it was shown how areas enclosed (1) between the value of controller output and its new steady value and (2) under the error curve itself (both versus time),can be expressed by very simple relations even when the control system is of high order. Later, the control area of the error curve has been utilized alone with more or less success in optimizing the control system [33,34]. Recently, interest has reawakened in this early work because of the rapid evaluation of discrete systems concepts.

The performance index now employed frequently in system optimization is really the area enclosed by more complex functions of the error signal vs. time, i.e. absolute value of error, square of error, square of manipulated variable of the process, and so on; but this makes the analysis more difficult.

The current work is based on the area enclosed between the normalized input and output curves of the process vs. time. It will be seen that this area has a definite physical meaning and can be used to advantage in controlling the process. Therefore, it will be called the control area of the process.

The assumptions for this investigation are:

1. The process is controllable, i.e. it must always be possible to bring the process to the desired steady state by adequate changes in input variable.

2. The process parameters are time variant, but with time constants which are longer than time constants which occur in the control transient itself.

3. The controlled process is a combination of physical processes capable of storing and giving up any kind of energy, as well as dissipating energy; and therefore, its dynamic performance can be approximated by an nth-order linear system or a second or third-order linear system together with time delay.

4. The time intervals between the significant disturbance changes is longer than the minimal time needed for the process performance identification.

Following these assumptions, changes of the process output c affected by an arbitrary input m(t) can be approximated by the differential equation:

$$A_n c^{(n)} + A_{n-1} c^{(n-1)} \ldots + A_2 \ddot{c} + A_1 \dot{c} + c = \mu m \tag{1}$$

At this time, we restrict ourselves to the case with simple forcing functions and the process which includes the term c in Eq. (1).

The input and output variables of the process have generally different physical natures. For example, very often the input variable is a control valve position and the output variable is the physical value to be controlled. The scale coefficient μ has to be selected so that $c = \mu m$ is on a common diagram for input and output variables in each steady state (i.e. normalized for unity steady state gain). Under these conditions the control area is shown in Fig. 27. This requires for each new control action a linear transformation of input variable coordinate system for an amount just sufficient to compensate for the effect of disturbance.

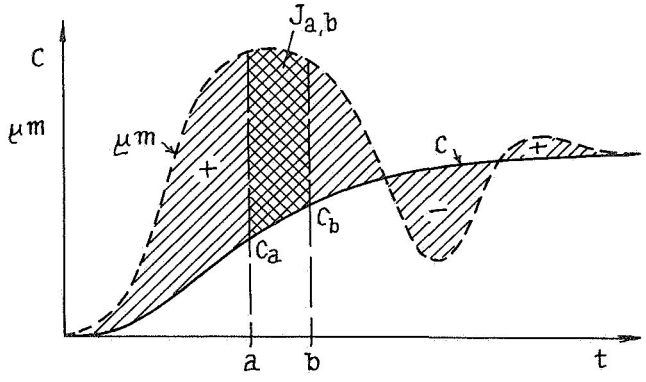

Fig. 27 The Control Area of the Process

μm - arbitrary change of process input variable

c - following change of process output

$J_{a,b}$ - control impulse in arbitrary time interval between a and b

Analogous to a mechanical system which describes the recti-linear motion of masses interconnected with the spring and placed in a resistant medium, under the action of an external force, the difference $\mu m - c$ can be taken as the control force. In Fig. 27 this is the difference of ordinates between the input and output curves.

For the case when the normalized input μm is changed from one steady value to another, the process parameter A_1 is directly associated with the final change, whereas the other process parameters A_2, A_3 . . . A_n are more strongly associated with transient energy storage effects. The process parameter, which is of the greatest interest here, is strongly related to energy dissipation effects throughout the process.

After rearranging Eq. (1), it may be integrated between the arbitrary limits a and b to give

$$\mu \int_a^b m dt - \int_a^b c dt = A_1(c_b - c_a) + A_2(\dot{c}_b - \dot{c}_a) + A_{n-1}[c_b^{(n-2)} - c_a^{(n-2)}] + A_n[c_b^{(n-1)} - c_a^{(n-1)}] \tag{2}$$

The difference between the two left-hand-side integrals represents the control area, and the terms on the right-hand-side reveal the relative importance of various higher derivative terms in contributing to the area.

The integral of the applied force in a definite time interval is called "force impulse" in mechanics. Similarly, for a process to be controlled, the control area determines the impulse of the control force transmitted to the process.

When the integration limits are extended from one steady state to another, a very important property of the control area is revealed. In this case, all derivatives of the controlled variable up to order (n-1) in both limit instances are zero, and Eq. (1) reduces to

$$\mu \int_0^\infty m dt - \int_0^\infty c dt = A_1(c_\infty - c_o) \tag{3}$$

This is the complete cross-hatched area in Fig. 27, and gives the impulse of the control force necessary to change the control variable by the amount $c_\infty - c_o$. In other words determining the control area is a means of experimentally determining the parameter A_1.

By integrating from some other initial time t_a one obtains

$$\mu \int_a^\infty m dt - \int_a^\infty c dt = A_1(c_\infty - c_o) - [A_2 \dot{c}_a + A_3 \ddot{c}_a \ldots + A_n c_a^{(n-1)}] \tag{4}$$

We see from this equation that it should be possible to measure c and its first n-1 derivatives for a process having known parameters A_1, A_2, etc. which is in some non-equilibrium state, and predict the control area needed to bring the process to a desired new steady-state. The input forcing function μm and the output c may have many different forms -- it is only necessary that the input eventually must attain a steady value and the area between the curves must equal the needed value.

Process Analysis During a Control Period

Equation (2) expresses the relation between a definite impulse of control force and corresponding changes of the controlled variable c from the value c_a to the value c_b, and of its derivatives from the values $\dot{c}_a$, $\ddot{c}_a$, . . . to the value $\dot{c}_b$, $\ddot{c}_b$, . . .

Therefore, this equation expresses the conditions of equality which must exist between the control force impulse during a time interval and the change occurring in the controlled variable c and its derivatives.

As in mechanics, the term "process momentum", may be used as the name for the product of the transient parameter A_2 and "velocity" c. Likewise, higher order "process momentum" terms could introduce the term result from taking the product of the transient parameter A_3 and the second derivative of the controlled variable, and so on.

The equation of equilibrium can be applied many times for many different intervals, and consequently, we may form a set of n+1 equations where $A_1 \ldots A_n$ and μ are the unknown process parameters to be determined.

For each time interval the left-hand-side of Eq. (2), the control impulse may be evaluated as the enclosed area between the curves for μm and c. The controlled variable c and its derivatives may be determined from measurements made at the sampling times.

The time derivatives we need for the process analysis can be practically measured or calculated up to the second order. This limits the process analysis to an equivalent third-order system.

This is sufficient because experience shows that the processes of very high order can be well approximated by a third-order linear system and an additional dead time T_d. Therefore, the process analysis can be generally evaluated by seeking its equivalent transfer function of the form

$$G(s)=\frac{\mu e^{-T_d s}}{(T^2 s^2+2\zeta T s+1)(Ts+1)} \qquad (5)$$

where ζ can be taken as a constant damping ratio for a definite process. This makes it possible to distinguish between processes which are highly damped ($\zeta>1$) from processes which are under damped ($\zeta<1$).

$$\left[\begin{matrix}\text{control impulse}\\ \text{between } (a-T_d) \text{ \& } (b-T_d)\end{matrix}\right] = T(1+2\zeta)(c_b-c_a) + T^2(1+2\zeta)(\dot{c}_b-\dot{c}_a) + T^3(\ddot{c}_b-\ddot{c}_a) \qquad (6)$$

For a second-order approximation the right-hand-side of Eq. (6) is

$$= T\zeta\,(c_b-c_a) + T^2(\dot{c}_b-\dot{c}_a) \qquad (6a)$$

From the values of c, $\dot{c}$, and $\ddot{c}$ at different sampling times these equations (6) and (6a) permit us to form a regularly updated computation of process parameters T and T_d. They will generally be very slowly changeable values. The process input signal synthesis that follows will always be based on the latest values contained in the computer memory.

The unknown scale factor μ which influences the control impulse will be simultaneously calculated and corrected at the same sampling times after each change of input variable. Its value defines the steady-state input variable needed to achieve the desired new steady output.

Computer Implemented Control

At this point we may begin to look at how the control area concept may be applied to a closed loop control system employing a digital computer.

For bringing a previously disturbed process to a desired steady state, the needed control area is defined by Eq. (4). In order to achieve a satisfactory response of the process, it will be necessary to change the process input variable at appropriate times.

Here we shall take for the best response the one with minimum time and no overshoot. Therefore, we will apply a modified minimum time concept for the input signal synthesis. Usually the minimum time response is evaluated for the case of a constant maximum process input undergoing only change of sign (bang-bang control). In the beginning the process input is applied with the sign needed to start the output with desired direction. At the "right" time the sign of the input is changed to bring the output to its new equilibrium value.

Starting from a physical viewpoint, we can define a different minimum response time concept for linear systems as the kind of control in which a "symmetrical" control impulse exchange occurs near the end of the control impulse exchange occurring immediately following a step input.

Fig. 28a shows the step response of a third-order process and how the components of the output, given by individual terms in the process differential equation, change their values with time. The area under $A_1\dot{c}$ represents the control impulse stored in the first and second-order process momentum terms defined earlier. Their sum as a function of time is given in the last diagram in Fig. 28a.

We obtain the condition for the desired net control impulse exchange by a "symmetrical" dissipation of individual terms representing the process differential equation, but in reverse order. This is shown in Fig. 28b, where it is interesting to see how the input signal μm must be programmed to force the desired net control impulse exchange. Again, the last row in Fig. 28 shows how the storage of control impulse changes with time.

Fig. 28c shows, by using a combination of beginning curves (Fig. 28a) and ending curves (Fig. 28b), how a desired response time can be obtained.

It is clear that this incorporation of beginning curves and ending curves is now always so simple to

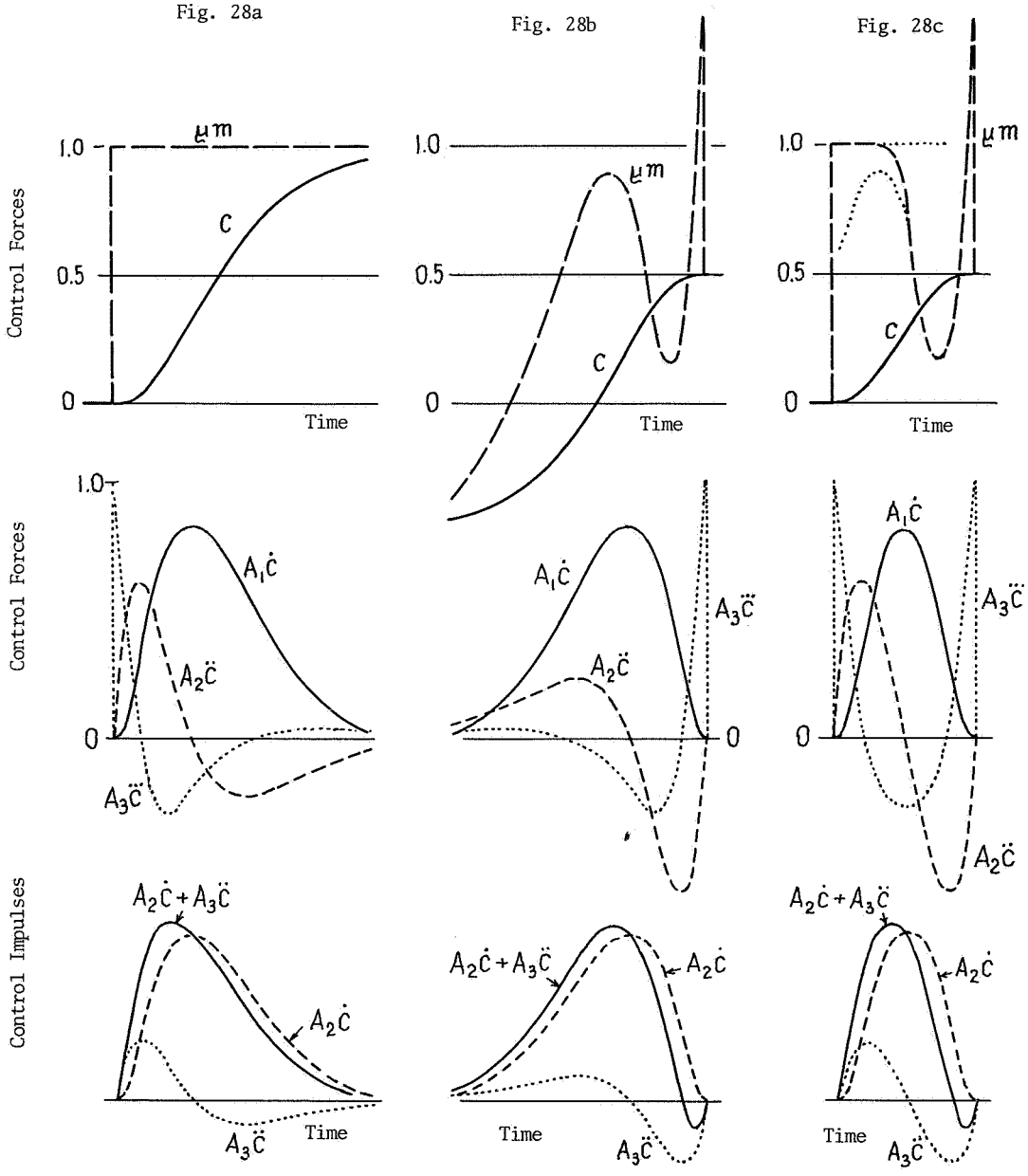

Fig. 28 Definition of a Linear Minimum Time Response Control

(a) Step Response for a Process Defined by Differential Equations $A_3\ddot{c} + A_2\ddot{c} + A_1\dot{c} + c = \mu m$

(b) Forced End of Control Transient for a Linear Minimum Time Response for the Same Process

(c) Idealized Linear Minimum Time Response for Changing the Controlled Variable from one Equilibrium Value to Another

Row 1 - Process Input-Output
Row 2 - Process Output Components
Row 3 - Control Impulse Storage in Process Momenta

realize, especially for high order processes. However, this is not so important, except in the case of changing from one equilibrium value of the controlled variable to another. The general case is much more interesting. Starting from a nonequilibrium process state with stored control impulse in the process, how can the controlled variable be brought to the desired value in minimum time? This means that within the limitations imposed on the maximum magnitude of the input signal (or on its rate of change) the control transient should not overshoot.

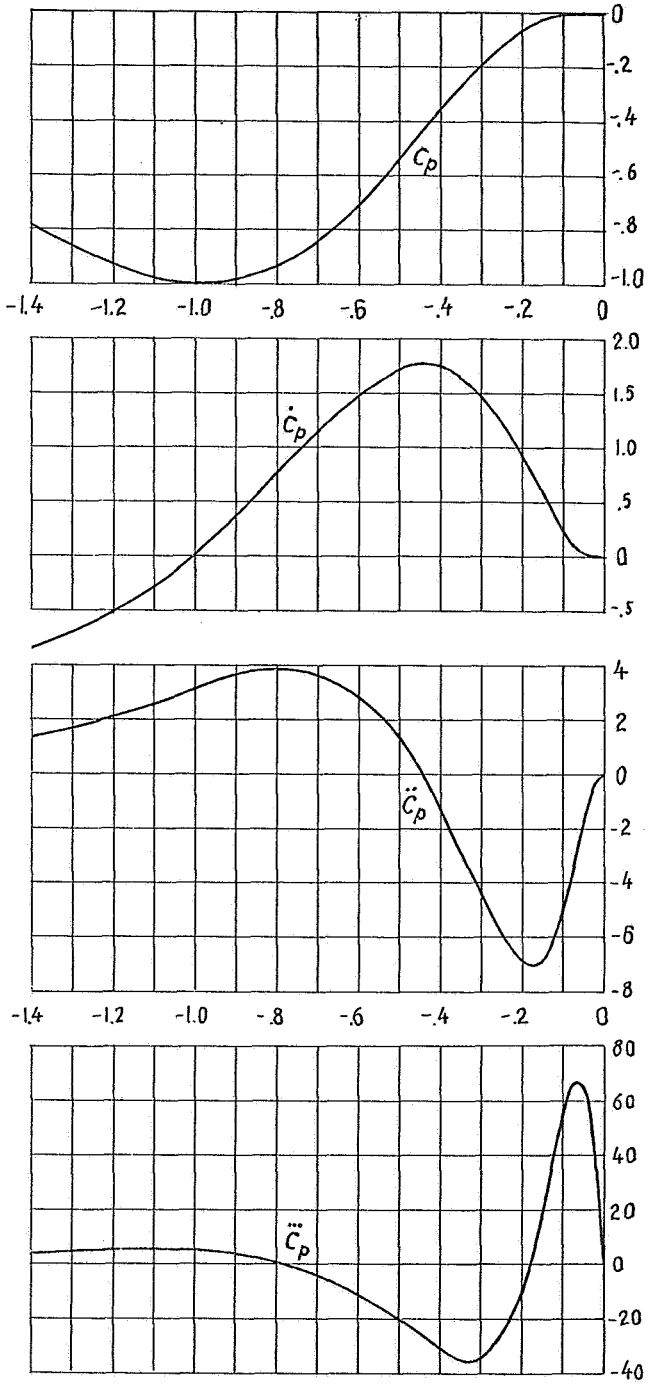

Fig. 29 A Set of Patterns for Ending a Control Transient in Minimum Time; Prepared for a Third-Order Process

This can be realized by applying the following procedure.

Intuitive patterns for the desired forced change of controlled variable with its calculated time derivatives is prepared as a model and inserted in the computer memory. These intuitive patterns are made up so that they would not require very large or very fast changes of the process input variable. Such a set of patterns is shown graphically in Fig. 29 and the block diagram for the proposed control method is shown in Fig. 30.

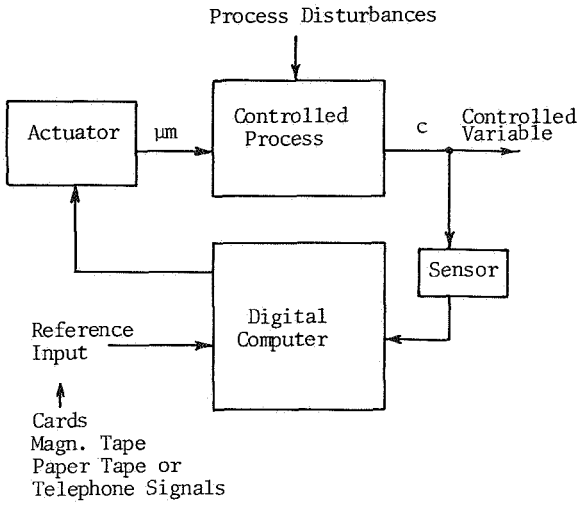

Fig. 30 Block Diagram for the Proposed Control Method

During the control transient for equal increments in time, and thus for each new process state, the corresponding instant in the model is sought. This instant in the model is found by varying the scale factors which connect the model values to that of the real controlled process. With the help of model values and process parameters the input signal can then be predicted.

The magnitude scale factor is the same for the variable as for all its derivatives, time scale factor is not. For example, if the time in the model must be multiplied by a factor τ to receive the corresponding instant in process, then the magnitude of the first derivative in the model must be multiplied by $1/\tau$, of the second by $1/\tau^2$, and so on, to receive the process derivatives.

At the same time the corresponding instant in model must satisfy the constraints that the process input variable has.

For a second-order process whose state is defined by the controlled variable and its first derivative, each instant during which the model shows the same sign for $\dot{c}$ as for c, the model can be applied, but only for one instant of time it will be possible for the model to satisfy the desired real input signal constraints.

For third-order process approximation and corresponding signs of derivatives only for one instant of time in the model is it possible to have the same time scale factors for the first and second time derivatives. If this instant predicts the values for the input signal which will not be within prescribed limits, a new instant of time in the model is then chosen so that the predicted process input lies within the physical limitations. Clearly, a scale compromise is made so that average values for the scale factors must be taken for the process input calculations.

The information so received about the process input for a definite controlled process state can be valid up to the end of control transient, but we use this information only for the next time interval. After each new increment of time a new input signal calculation for the changed controlled process state will predict an improved input signal. Thus, always repeating the same calculation and using the latest values for the process analysis, the input signal will be predicted with sufficient accuracy to bring the controlled process to the desired steady state in practically a minimum time.

For the processes having the approximation parameters with a dead time T_d, the calculated input must be advanced in time by T_d.

The values so received for the process input signal are applied only as a basis for the necessary control area calculations. This technique permits an additional transformation of input signals with high peak magnitudes or speeds to reasonable values but having the same impulse of control force in definite time intervals.

Finally, it must be mentioned that the computation technique is guided by control logic. After the disturbance, depending on controlled variable error, sign and magnitude of derivatives, the control logic changes the process input variable by an amount just sufficient to start a fast control impulse exchange with the controlled process. The control logic decides about the amount of control impulse which can be temporarily stored in the controlled process, i.e., about the instant when the program for taking away the control impulse stored in the process momenta must start. Furthermore, for each definite combination of signs for the controlled variable and its derivatives, the control logic finds the corresponding region for the corresponding instant in the model.

PARTICIPATION IN IFAC FLUIDICS SYMPOSIUM IN LONDON, ENGLAND NOVEMBER 1968

J. L. Shearer, Rockwell Prof. of Engineering

The final symposium sponsored by the IFAC Technical Committee on Components in 1968 was the Fluidics Symposium, held in London 3-8 November. Of the 156 registrants from 14 countries, only about 145 attended this symposium of six sessions, containing 25 papers, devoted to various aspects of fluidics. The main topics under which the topics were arranged were: Fluid Mechanics, Component and Systems Design, Applications, and General. Among the missing persons were delegates from Poland and Russia whose papers were presented by delegates from the host country.

The highlights of the technical program included papers dealing with various aspects of jet deflection in fluid amplifiers, recent work on vortex amplifiers and impact modulators, miniaturization through the use of low Reynolds no. flows, fluid amplifier controlled artificial heart system, a fluidic pressure racial sensor for gas turbine engine control, operational characteristics of a curved wall fluid amplifier, and dynamic analysis of a Tesla Diode.

This symposium was organized under the auspices of the Royal Aeronautical Society, and it was held in their headquarters building in London. All of the arrangements were carried out in an excellent manner, and preprints of all papers including an excellent survey of the Third Cranfield Conference on Fluidics (Torino, 8-10 May 1969) were provided. Prof. J.K. Royle served as chairman of the Organizing Committee and Dr. A. M. Ballantyne, secretary of the Royal Aeronautical Society, made available the fullest possible use of the facilities of the RAS. Profs. G. D. S. Maclellan and K. Foster also contributed very effectively to the overall operation of the symposium.

Because of the need to help represent the United States at the IFAC Paper Selection Committee meetings in Warsaw during the latter part of the week, the author was not able to attend the sessions on the last dav.

The Proceedings are available at a cost of about $25 from: Secretary, Royal Aeronautical Society, 4 Hamilton Place, London W1V, OBQ, England.

For further information about the projects mentioned in this report of the activities of the Systems and Controls Laboratory, inquiries should be addressed to: Director, Systems and Controls Laboratory, 214 Mechanical Engineering Building, University Park, Pa. 16802.

LIST OF REFERENCES

1. Research Report No. 1, Systems and Controls Laboratory, The Pennsylvania State University, April 1965.

2. Research Report No. 2, Systems and Controls Laboratory, The Pennsylvania State University, October 1965.

3. Research Report No. 3, Systems and Controls Laboratory, The Pennsylvania State University, April 1966.

4. Research Report No. 4, Systems and Controls Laboratory, The Pennsylvania State University, October 1966.

5. Research Report No. 5, Systems and Controls Laboratory, The Pennsylvania State University, April 1967.

6. Research Report No. 6, Systems and Controls Laboratory, The Pennsylvania State University, October 1967.

7. Research Report No. 7, Systems and Controls Laboratory, The Pennsylvania State University, April 1968.

8. Research Report No. 8, Systems and Controls Laboratory, The Pennsylvania State University, October 1968.

9. Effects of Upstream Disturbance Intensity on the Spreading of a Semi-Confined Jet, Gray, R. W., M.S. Thesis, The Pennsylvania State University, June 1969.

10. "The Effect of Initial Conditions on the Development of a Free Shear Layer", P. Bradshaw, Journal of Fluid Mechanics, Vol. 26, p. 225, 1966.

11. "Secondary Flow Effects in a Bounded Rectangular Jet", Foss, J. F., and Jones, J. B., ASME Paper No. 68-FE-17.

12. Experimental Study of Spreading of Semi-Confined Jets, R. Bettoli, M.S. Thesis, The Pennsylvania State University, December 1967.

13. Thermal Separation Control Applied to Electro-Fluidic Switching in a Straight-Walled Diffuser, R. E. Tomek, Ph. D. Thesis, The Pennsylvania State University, September 1968.

14. Variable Area Flowmeter Handbook, Fischer and Porter Co., Warmister, Pa., Vol. 2, May 1968.

15. Fluid Power Control, Blackburn, J. F., Reethof, G., and Shearer, J. L., The M.I.T. Press, Cambridge, Mass. 1960.

16. Matheson Gas Data Book, Fourth Ed., Matheson Canada Ltd., Witby, Ontario, Canada, 1966.

17. Static and Dynamic Modeling of a Pressure-Controlled Subsonic Fluid Jet Modulator, R. J. Gurski, Sc.D. Thesis, Massachusetts Institute of Technology, May 1965.

18. The Structure of Turbulent Shear Flow, A. A. Townsend, Cambridge University Press, p. 91, 1956.

19. "Fluid Transmission Lines", K. N. Reid, Special Class Notes written at Oklahoma State University in 1966 (copies may be obtained by writing to K. N. Reid, Dept. of Mechanical Engineering, Oklahoma State University, Stillwater, Okla.)

20. "An Evaluation of the Hydrogen Bubble Technique for the Quantitative Determination of Fluid Velocities within Clear Tubes", Davis, W. and Fox, R. W., Trans. ASME, Journal of Basic Engineering, Vol. 89, pp. 771-781, Dec. 1967.

21. "Adaptive Control for Prime Movers", P. H. Schweitzer, C. Volz, and F. DeLuca, ASME Paper 67 WA/DGP-2.

22. "Optimizing Control of Single Input Extremum Systems", J. S. Frait and D. P. Eckman, Journal of Basic Engineering, Vol. 84, pp. 85-90, March 1962.

23. "General Stability Analysis of Sinusoidal Perturbation Extremum Searching Adaptive Systems", V. W. Eveleigh, Proceedings of the Second IFAC Congress, pp. 472-480, 1963.

24. "Development of a Digital Fluidic Optimizer", V.K.B. Lehtinen, P. A. Orner, Preprints of Fourth IFAC Congress, 1969.

25. "Variable Frequency Electric Circuit Theory", J. R. Carson and T. C. Fry, Bell System Technical Journal, Vol. 16, pp. 513-540, 1937.

26. "The Fundamental Principles of Frequency Modulation", B. Van der Pol, Proc. I.E.E., Vol. 93, Pt. III, pp. 153-158, 1946.

27. "Transmission of F. M. Signals Through Linear Filters", D. T. Hess, Proc. Nat. Electronics Conf., pp. 469-476, 1962.

28. "A Fluid Amplifier Technique for Speed Governing Using Carrier Frequency Modulation", W. A. Boothe, C. G. Ringwall, and L. R. Kelley, Paper No. 31G presented in London at IFAC Meeting on Fluid Logic and Control Devices, 23 June 1966.

29. Information Transmission, Modulation and Noise, M. Schwartz, McGraw-Hill, 1959.

30. "Vent Effects in the Response of a Proportional Fluid Amplifier", A. J. Healey, Trans. A.S.M.E. Journal of Basic Engineering, Vol. 90, No. 1, pp. 90-96, 1968.

31. "Dynamic Response of Analog Fluid Amplifiers", A. J. Healey, Proceedings of Symposium on Fluidics and Related Internal Flows, The Pennsylvania State University, pp. 77-104, Oct. 1968.

32. "Die Abweichungstlaeche bei Schnellreglervorgaengen", I. Obradovic, Archiv fuer Elektrotechnik, pp. 382-390, 1942.

33. The Dynamics of Automatic Controls, R. Oldenburg, H. Sartorius, A.S.M.E., New York, 1948.

34. "A Note on Control-Area", T. M. Stout, J. of Applied Physics, pp. 1129-1131, Nov. 1950.